A coupled Thermo-Hygro-Chemical model for characterising autogenous healing in ordinary cementitious materials

Adriana Silviana Chitez[a],
Anthony Duncan Jefferson[a], *

[a]Cardiff University, School of Engineering, Queen's Buildings, The Parade CF24 3AA, UK, www.cardiff.ac.uk

* Corresponding author. JeffersonAD@cardiff.ac.uk (A.D. Jefferson)
Tel.: +44 (0)29 20 865697

Abstract

Experimental work has demonstrated that cracks can be healed in ordinary cementitious materials in the presence of water. The primary healing mechanisms are hydration of the unreacted nuclei of cement particles and the long-term formation of calcite. A mathematical model for simulating early-age autogenous healing of ordinary cement-based materials is proposed, which employs a coupled thermo-hygro-chemical (THC) framework and which uses a reactive water transport component to predict the movement of healing materials. A single concentration variable is employed for the healing component of the model that is derived directly from the quantity of unreacted cement and computed using a generalised cement hydration model component. The hydration component is directly linked to an expression for capillary porosity and for the porosity of the material within a healed crack. The results from a series of model simulations are in good general agreement with experimental data from tests on autogenous healing.

Nomenclature

a	material parameter	K_X	order of reaction of mineral X
a_i	constant; $i \in [1,5]$	m	material parameter
A_k, A_Γ	material parameters	m_i	mass of i per unit volume [kgm^{-3}]
A_p, A_w			
A_λ	material parameters [K^{-1}]	$\dot{m}_\pi^i$	type i mass rate of phase π [kgm^{-3}s^{-1}]
A_{crack}	area under the crack width curve [μm^2]	mc_i	type i moisture content

b	material parameter
b_i	constant; $i \in [1,5]$
B_v	material coefficient
c_1, c_2	empirical constants
c_{FA}	porosity coefficient due to FA
$c\eta$	material parameter
$\hat{\boldsymbol{C}}$	global secant capacitance matrix
$C^i_{\eta S}$	material coefficient of porosity type i
C^{π}_p	specific heat capacity of π [$JK^{-1}kg^{-1}$]
d_{cz}	porosity material coefficient in crack zone
D^i_{π}	type i diffusion coefficient of π [m^2s^{-1}]
E	activation energy of the reaction [$Jkmol^{-1}$]
f_i	weight ratio of i in terms of total cement content [%]
f_s	structure coefficient
$\hat{\boldsymbol{F}}$	global right-hand side vector
$\overline{g}$	gravity vector [ms^{-2}]
H_i	total heat of hydration of material i [Jm^{-3}]
$\boldsymbol{J}^i_{\pi}$	type i flux of phase π [$kgm^{-2}s^{-1}$]
k^i_{π}	type i permeability coefficient of π [m^2]
$\hat{\boldsymbol{K}}$	global secant hydraulic conductivity matrix
M_w	molar mass of the water [$kgkmol^{-1}$]
ne	number of finite elements
nn	number of nodes
$\overline{n}$	unit normal vector
$\boldsymbol{N}$	vector of shape function
p_i	pressure type i [Pa]
q_{π}	imposed flux of phase π [$kgm^{-2}s^{-1}$;$Jm^{-2}s^{-1}$]
Q_h	rate of heat generation [$Jm^{-3}s^{-1}$]
R	ideal gas constant [$JK^{-1}kmol^{-1}$]
RH	relative humidity
R_{ck}	average radius of the clinker grain [m]
S_{π}	saturation degree of phase π
t	time [s]
T	temperature [K]
$\overline{v}^{ws}$	mass-averaged velocity of water phase with respect to solid phase[ms^{-1}]
V_i	volume of i per unit volume [m^3m^{-3}]
w_{crack}	crack width [µm]
w_{ref}	reference crack width [µm]
w^{ult}_i	ultimate quantity of the gel water i [kgm^{-3}]
w/c	water-cement ratio

Greek symbols

α	empirical constant
α_{Lg}	longitudinal dispersivity coefficient [m]
α_P	precipitation parameter
β	hydration shape parameter
β_{Tr}	transversal dispersivity coefficient [m]
β_P	precipitation parameter
γ	filling fraction
γ_{norm}	normalized filling fraction
Γ	degree of hydration
Γ_q	boundary of the domain
δ_{ij}	Kronecker delta
δ_T	heat transfer coefficient [W m^{-2} K^{-1}]
δ_{wv}	moisture transfer coefficient [m s^{-1}]
δ_{ω}	solute transfer coefficient [kg s^{-1} m^{-2}]
$\delta\boldsymbol{\Phi}$	increment of the vector of unknowns
ΔH_v	specific heat of evaporation [J kg^{-1}]
Δt	time increment [s]
η	porosity
κ_X	rate constant of the mineral X
λ^{eff}_{dry}	effective thermal conductivity of a dry material [W K^{-1} m^{-1}]
μ_w	dynamic viscosity of liquid water [µPa s]
ρ_{π}	density of phase/material π [kg m^{-3}]
$\overline{\rho}_{\pi}$	phase-averaged density of π [kg m^{-3}]
$\overline{\rho C}_p$	storage heat capacity [J m^{-3} K^{-1}]
τ	hydration time parameter
$\boldsymbol{\Phi}$	vector of unknowns
$\boldsymbol{\Psi}$	residual vector
ω	mass of unreacted cement per mass of capillary solution [kg kg^{-1}]
Ω	domain

Subscripts/superscripts-

agg	aggregate	eff	effective value	P	precipitate
atm	atmospheric	$endST\,1$	end of stage 1	ref	reference value
A	advective	env	environmental value	rel	relative value
AW	adsorbed water	FA	fly ash	res	residual value
cap	capillary	g	gas	s	solid
cem	Portland cement	$GGBF$	ground-granulated blast-furnace slag cement	sat	saturated value
$clink$	clinker	hyd	hydration	str	strain
cr	critical value	int	intrinsic value	SCM	supplementary cementing materials
cz	crack zone	int_{mat}	intrinsic value of the matured paste	SGW	small gel water
CBW	chemically combined water	I	end of the induction period	tot	total
CD	conductive	IGW	intraglobular water	T	temperature
CW	capillary water	ILW	interlayer water	ult	ultimate value
da	dry air	k	iteration number	UCP	unreacted cement paste
des	desorption	LGW	large gel pore water	v	water vapour
dry	dry condition value	mol	molecular	w	liquid water
D	diffusive	n	step number	wv	moisture
DD	diffusive-dispersive	NG	end of the nucleation and growth controlled period	ω	solute
e	elemental value	per	percolation threshold of Γ	0	initial value
ea	entrapped air	pm	porous material		

Notations

•	time derivative of X	$\frac{D^s}{Dt}$	material time derivative with respect to the solid phase	div	divergence operator (spatial description)
		$\frac{\partial}{\partial X}$	partial derivative with respect to X	$grad$	gradient operator (spatial description)

1. Introduction

Cementitious composites are quasi-brittle materials that develop their porous internal micro-structure during hydration. The complex pore structure within these materials, along with any micro-cracks present, largely governs the moisture and heat transfer properties of the composite material. Structures formed from these cementitious materials have frequently suffered from poor durability that has resulted in expensive repair and maintenance work. In recent years, researchers have investigated new cementitious materials that have the ability to self-repair, as a possible remedy to these durability problems.

Since Turner's first discussion on crack repair [1], the pace of experimental research on self-healing in cementitious has greatly accelerated [2-4]. Van Tittelboom and De Belie [2] provided an extensive state-of-the-art review of research on self-healing in cementitious

materials in which the authors identified two main groups of self-healing techniques: (i) ‘autonomic’ healing, in which a single or multi-component healing agent is released from embedded capsules or vascular systems by damage and temperature activation [3] and (ii) ‘intrinsic’/ ‘autogenic’ self-healing, based on the chemical reactions between the components of the cementitious matrix. In the latter case, the recovery of mechanical or durability properties is obtained either by autogenous healing or by healing in a polymer modified concrete [2]. Initially, autogenous healing was attributed solely to ongoing hydration of the remnant clinker and intercrystallisation of the fractured crystals [1]. More recent research suggests that continuous hydration is only predominant in the first weeks after casting, when the amount of unreacted cement is significant, but that calcite formation is the main mechanism thereafter [2,4–6]. Experimental tests showed a decrease of water permeability, a recovery of stiffness and a regain of compressive and flexural strengths [4–11]. The number of numerical studies on autogenous healing is still limited. Ter Heide [12] incorporated the bar and ribbon models developed by Lokhorst [13] and Koenders [14] and used bridging particles to fill the existing gaps between the clusters of hydrates formed as a result of the expansion of unhydrated cement. The distribution and further hydration of these particles were simulated considering diffusion and thermodynamic principles in the HYMOSTRUC [15] model. Huang and collaborators proposed an alternative modelling approach for autogenous healing in high performance concrete [16]. Again, the distribution and fraction of the unreacted cement particles were determined with the microstructural model HYMOSTRUC 3D. This time though, the dissociated ions from the clinker minerals were transported to the crack surface via a diffusion model, while the precipitation of the hydrates was represented in a thermodynamic model comprising mass and charge balance as well as chemical equilibrium. The mechanical recovery of the cracked cement paste was investigated using finite element models by Remmers and de Borst [17] and Hilloulin et al. [18]. Remmers and de Borst introduced momentum and mass balance equations for a fluid-saturated porous medium and modelled crack rebonding by adding a strength and stiffness increment of the interface to the constitutive relation that governs the crack opening. Hilloulin et al., on the other hand, solved a hydro-chemo-mechanical problem in which the chemical reactions were simulated in a hydration model based on the Arrhenius law.

In this paper a numerical study is presented on the simulation of autogenous healing of young cement-based materials. Dissolved clinker is modelled as a single solute that can be diffused and advected due to concentration and water pressure gradients, respectively. The thermo-hygral model formulated for transport phenomena in a porous medium [19,20] has been extended with a mass balance equation for the healing product. The kinetics of phase change, from dissolved clinker to precipitated material, is modelled using Freundlich

equilibrium isotherm. The formation and variation of the porous network before and during crack recovery is assessed using the microstructural model STOICH_HC2 [21,22]. The model is validated using data from recent tests undertaken at Cardiff University as well as from autogenous healing experiments reported in the literature. As discussed more fully in section 3, the authors consider that the efficiency of this semi-phenomenological model would allow it to be coupled to a mechanical analysis and employed in the analysis of full-scale structures. The assumptions upon which the model is based means that is more applicable to early age self-healing than to long-term calcite formation.

2. Structure of the hydrated cement

The hydration of cement based materials leads, in the early stages of the reaction, to the appearance of an unstable chemical system with varying physical and chemical properties.

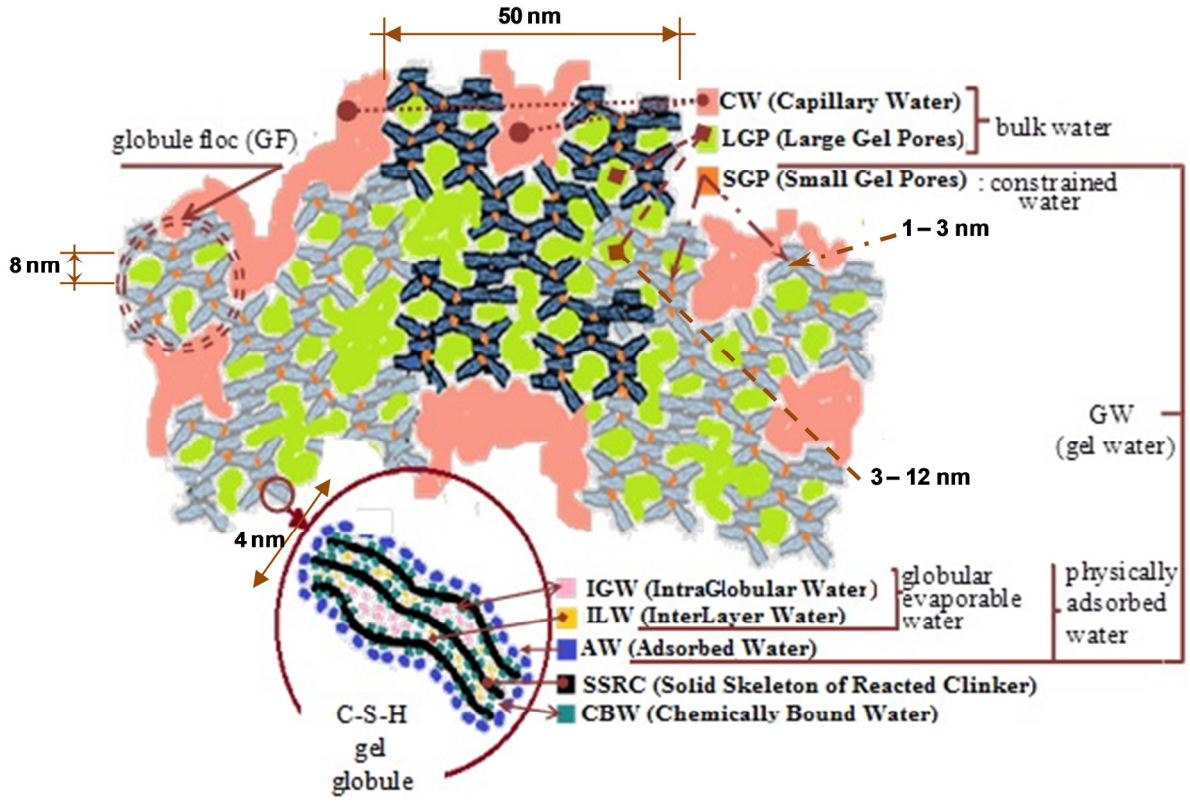

Figure 1 Water forms within the calcium silicate hydrate gel

In the current investigation, the microstructural model STOICH_HC2 [21,22] is adopted to trace the hydration kinetics of Portland cement. This model, based on Jennings' description [23] of the calcium silicate hydrate ($C-S-H$) gel, which is depicted here in Figure 1, takes into account the quantitative evolution of the mix constituents, the transformation of the porous network and the chemical shrinkage. According to Jennings, Portland cement

behaves as a colloidal material due to the existence of various water forms. Its gel-like structure comprises:

- Ca^{2+}, Si^{2+} and O^{2-} ions that form the solid skeleton of the reacted clinker (SSRC);
- chemically bound water (CBW) strongly attached to the solid skeleton;
- intraglobular, interlayer and adsorbed water (IGW+ILW+AW);
- water in small gel pores (SGW) encapsulated between the silicate globules and
- water in large gel pores (LGW) that separate two neighbouring globule flocs.

The above morphological description contradicts the recent work of Müller et al. [24–26] that found only two nanoscale pore sizes associated with the calcium silicate hydrate. Their ^{1}H nuclear magnetic resonance (NMR) relaxation tests revealed the fact that the large gel pores reported by Jennings do not seem to be an intrinsic part of the $C-S-H$. In spite of this, the validity of our work does not depend on the veracity of these NMR determined measurements. The authors acknowledge that if compatibility with Müller et al.'s results is sought, the classification of our 'grouped' water forms and their corresponding relative humidity boundaries, mentioned below, would need to be altered.

In STOICH_HC2 it is assumed that the sequential desorption of LGW, SGW and IGW+ILW+AW occurs during three humidity ranges: [60%, 40%), [40%, 11%) and [11%, 0%) [23,27,28] which are demarcated in terms of water content by four water mole thresholds. Therefore, the gel liquid phases and the capillary water (CW) are quantified by solving iteratively the chemical reactions listed in Annex A, Table A. 1 using the four sets of stoichiometric coefficients from Table A. 2. A brief description of the computational procedure is presented below, but more details can be found in [21,22].

The reaction kinetics encompass three main stages: (i) the induction period, (ii) the nucleation and growth stage and (iii) the diffusion controlled hydration [29,30]. The general form of the corresponding individual hydration curves is given in equation (1), whilst the values of the hydration parameters are provided in Annex A, Table A. 3.

$$\Gamma_X(t)=\begin{cases}\dfrac{\Gamma_X^I}{t_X^I}t & ,\forall t<t_X^I \\ \Gamma_X^I+1-\dfrac{1}{\exp\left[\kappa_X\dfrac{\left(t-t_X^I\right)}{3600}\right]^{K_X}} & ,\forall t_X^I\le t<t_X^{NG} \\ 1-\left(-\dfrac{\sqrt{2D_X}}{R_{ck}}\sqrt{t-t_X^{NG}}+\sqrt[3]{1-\Gamma_X^{NG}}\right)^3 & ,\forall t\ge t_X^{NG}\end{cases} \quad ;X=\begin{array}{l}C_3S\text{ (alite)},\\ C_2S\text{ (belite)},\\ C_3A\text{ (aluminate)}\\ C_4AF\text{ (aluminoferrite)}\end{array} \tag{1}$$

For each time step, the quantities of clinker and water phases consumed during the hydrolysis are determined using equation (1). The masses of LGW, SGW, GW+ILW+AW and CBW per unit volume of material are then computed from $w_{60\%}$, $w_{40\%}$, $w_{11\%}$, $w_{0\%}$, which are the masses of the depleted water within the boundaries of the above mentioned humidity intervals:

$$\begin{aligned} w_{LGW}(t) &= w_{60\%}(t) - w_{40\%}(t) & \qquad w_{SGW}(t) &= w_{40\%}(t) - w_{11\%}(t) \\ w_{IGW+ILW+AW}(t) &= w_{11\%}(t) - w_{0\%}(t) & \qquad w_{CBW}(t) &= w_{0\%}(t) \end{aligned} \tag{2}$$

The microstructural model also predicts the ultimate hydration degree. This parameter is computed as the ratio between the effective water-cement ratio and the lowest water-cement ratio that would permit complete hydration [31]:

$$\Gamma_{ult} = \frac{w/c}{\frac{w_{0\%}}{c}} \leq 1 \tag{3}$$

3. Governing equations

Assuming that the gas remains constant at atmospheric pressure [32] and that the mechanical component does not significantly affect the thermo-hygro-chemical behaviour of the material, three macroscopic equilibrium equations are derived from the *volume averaging theorem within the hybrid mixture theory* [33,34]*:*

$$\frac{D^s\overline{\rho}_w}{Dt} + \frac{D^s\overline{\rho}_v}{Dt} + div\left(J_w^A\right) + div\left(J_v^D\right) = -\dot{m}_w^{hyd} - \dot{m}_w^{agg} + \dot{m}_w^{des} \tag{4}$$

$$\overline{\rho C}_p \frac{D^s T}{Dt} - div\left(J_T^{CD}\right) + \left(\dot{m}_v \Delta H_v - Q_h\right) = 0 \tag{5}$$

$$\text{where } \dot{m}_v = \dot{\overline{\rho}}_w + div\left(J_w^A\right) + \dot{m}_w^{hyd} + \dot{m}_w^{agg} - \dot{m}_w^{des}$$

$$\frac{D^s\overline{\rho}_\omega}{Dt} + div\left(J_\omega^A\right) + div\left(J_\omega^{DD}\right) = -\dot{m}_\omega \tag{6}$$

In the mass balance equations (4) and (6) the transfer of moisture and solute is assumed to take place in the capillary pore network. Thus, the averaged densities of water, water vapour and solute are equal to:

$$\overline{\rho}_w = \eta_{cap} S_w^{cap} \rho_w \qquad \overline{\rho}_v = \eta_{cap} S_g \rho_w;\ S_g = 1 - S_w^{cap} - S_P \qquad \overline{\rho}_\omega = \omega \eta_{cap} S_w^{cap} \rho_w \tag{7}$$

The equilibrium equations are formulated based on the work of Gawin and co-authors [20,35], that can be regarded as standard for such models. The constitutive laws employed are briefly enumerated in Table B. 1 together with the material parameters valid in the current investigation for all the numerical examples.

Regarding the three sink/source terms found in the right-hand side part of equation (4):

- $\dot{m}_w^{hyd}$ accounts for the rate of water consumed during the hydration process and is computed using the stoichiometrically determined water forms:

$$\dot{m}_w^{hyd} = \sum_i \left(w_i^{ult}\right) \cdot \dot{\Gamma}\,; \quad i \in \{SGW, IGW + ILW + AW, CBW\} \tag{8}$$

- $\dot{m}_w^{agg}$ represents the rate of absorption/desorption by the aggregate and is given by:

$$m_w^{agg}(t) = mc_{sat}\left\{mc_0 + \left[\left(mc_r - mc_0\right) + \alpha \exp\left(-c_1 \frac{t}{t_{sat}}\right)\right]\left[1 - \exp\left(-c_2 \frac{t}{t_{sat}}\right)\right]\right\} \tag{9}$$

where the parameters equal to: mc_{sat} = 0.578, mc_r =0.5, mc_0 = 0, t_{sat} = 1, c_1 = 0.5, c_2 = 2.178 and α = 1.035 [22];

- m_w^{des} is the rate by which the capillary network is supplied with aqueous phase from the gel pores when the inner relative humidity drops below the critical value of 40% [23,36,37]. The mass of gel water to be supplied equals:

$$m_w^{des} = \begin{cases} \dfrac{\partial\left(\eta_{cap} \dfrac{\rho_w}{V_{tot}} S_w^{cap}\right)}{\partial RH} & ,\forall RH \le RH_{cr} \\ 0 & ,\forall RH > RH_{cr} \end{cases} \tag{10}$$

In the enthalpy balance equation (5), all the phases existing in the porous material contribute to the heat capacity, as follows:

$$\overline{\rho C}_p = \sum_\pi \left(\overline{\rho}_\pi C_p^\pi\right); \quad \pi \in \{s, w, g\} \tag{11}$$

The rate of heat generation, Q_h, is determined using the relationship:

$$Q_h = H_{tot} \frac{d\Gamma}{dt} = H_{tot} \dot{\Gamma} \tag{12}$$

in which: the total heat release at complete hydration equals [38]:

$$H_{tot} = \sum_i \left(H_i f_i\right) \sum_i f_i\,; \quad i \in \{cem, GGBC, FA\} \tag{13}$$

and the hydration rate, $\dot{\Gamma}$, which represents the summation of the hydration rates of the different cement compounds, is computed from the STOICH_HC2 model.

The development of the porous network is influenced in the current model by both the hydration degree and the volume of material that precipitates during self-healing. Using the principles of Powers' model [27,39] and the stoichiometric algorithm STOICH_HC2, the following porosity function is used within the cementitious material:

173

$$\eta_i^{pm}(\Gamma,V_P)= \begin{cases} \dfrac{m_w-\Gamma\cdot c_{FA}^i\sum_i w_i^{ult}}{m_w-\Gamma_0\cdot c_{FA}^i\sum_i w_i^{ult}}\eta_i^{pm}\left(\Gamma_{per},V_P\right) & ,\forall\Gamma<\Gamma_{per} \\ \dfrac{\dfrac{m_w}{m_{cem}}+\dfrac{\rho_w}{m_{cem}}V_{ea}-\left[V_{str}(\Gamma)\dfrac{\rho_w}{m_{cem}}+\Gamma\cdot c_{FA}^i\left(C_{\eta S}^i+\dfrac{\rho_w}{m_{cem}}V_P\right)\right]}{\dfrac{\rho_w}{\rho_{cem}}+\dfrac{m_w}{m_{cem}}+\dfrac{\rho_w}{m_{cem}}\left(V_{ea}+\sum V_{agg}+\sum V_{SCM}\right)} & ,\forall\Gamma\geq\Gamma_{per} \end{cases} \qquad i\in\{cap,tot\} \tag{14}$$

174 in which the percolation hydration degree Γ_{per} equals 0.1 and $C_{\eta S}^i$ has the expression:

$$C_{\eta S}^{cap}=\frac{\rho_w}{m_{cem}}\sum_i\frac{w_i^{ult}}{\rho_i};\ i\in\{SGW,IGW+ILW+AW,CBW\} \qquad C_{\eta S}^{tot}=\frac{\rho_w}{m_{cem}}\frac{w_{CBW}^{ult}}{\rho_{CBW}} \tag{15}$$

175
176 In the crack zone, on the other hand, the porosity develops according to:

$$\eta_i^{cz}(\Gamma,V_P)=1-\frac{V_P}{V_{cz}}\left(1-d_{cz}\eta_i^{pm}(\Gamma,V_P)\right);\quad i\in\{cap,tot\} \tag{16}$$

177 where d_{cz} is a coefficient that increases the porosity of the deposited material based on a
178 locally higher water-cement ratio. It is clear that when transported material is first
179 precipitated, the water cement ratio is extremely high, if based on the total amount of water
180 in a crack. Therefore an assumption is needed that gives a realistic w/c ratio that results in
181 a material with, initially, a relatively high but realistic porosity. This constant (d_{cz}) is
182 calibrated using data from the first example and then adjusted accordingly for the other
183 examples. At present, back-calibration is our only means of identifying this constant, due to
184 the lack of the extremely detailed experimental data that would be required to measure its
185 value independently.

186 Returning to the mass balance equation (6), the sink source term $\dot{m}_\omega$ accounts for
187 autogenous healing which, from the chemical point of view, represents an interaction
188 between the liquid phase containing various dissociated ions from the unreacted cement and
189 the solid compounds. The dissolution of the clinker minerals leads to the supersaturation of
190 the aqueous phase with respect to the hydrates and is followed by precipitation from
191 solution. In general, these types of reactions are well modelled using the thermodynamic
192 principles. However, in the case of cement science, the available database from
193 geochemical systems cannot be used since it does not contain sufficient information for the
194 relevant solids and aqueous species. The addition of the missing data is an extremely
195 challenging task, as discussed in [40], because both the experimental and numerical
196 determination of the solubility of the clinker minerals has several limitations. For this reason,
197 a simplified approach, which assumes thermodynamic equilibrium between precipitated and

dissolved chemical products, was investigated in the current research to simulate the overall formation and accumulation of hydrates in the crack. A Freundlich type isotherm, which according to Chen et al. [41] is widely used to describe the adsorption of solutes in solution by solid phases, was preferred and employed. This approach was also presented in [42,43] to model salt ($NaCl$) precipitation/dissolution process in mortars. The isotherm given in (17) links the degree of pore saturation with precipitated salt, S_p, to the concentration of dissolved clinker, ω:

$$S_p = \alpha_P S_w^{cap} \omega^{\beta_P} \tag{17}$$

This relationship, in which α_P depends on the binder composition of the cement-based material and β_P represents the order of the chemical process, is used to obtain the expression of m_ω as follows:

$$m_\omega = \left(\alpha_P S_w^{cap} \omega^{\beta_P}\right) \rho_w \eta_{cap} \tag{18}$$

At the initiation of the autogenous healing process, the starting value of ω is computed as a mass ratio between the existing unhydrated cement and the effective capillary water:

$$\omega_0 = \frac{m_{UCP}}{m_{CW+LGW}} \tag{19}$$

where the mass of effective capillary water, m_{CW+LGW} , is given by the expression:

$$m_{CW+LGW} = m_{CW}^{ult} + \left(m_w - m_{CW}^{ult}\right)\frac{\left(\Gamma_{ult} - \Gamma_{endST1}\right)}{\Gamma_{ult}} + m_{LGW}^{ult}\frac{\Gamma_{endST1}}{\Gamma_{ult}} \tag{20}$$

This initial concentration is calculated assuming that during the induction period of cement hydration, a semipermeable layer of $C-S-H$ forms around the C_3S grain [44,45]. The transport of Ca^{2+} and OH^- between the grains and the pore solution is permitted, but the release of the larger silicate anions is hindered until the osmotic pressure, that builds up during the preferential diffusion, breaks down the protective layer. Therefore in order to account for this effect in the proposed numerical investigation, a reduction coefficient n_{UCP} is applied to the overall initial available mass of unreacted clinker, as can be seen in equation (21):

$$m_{UCP} = n_{UCP}\left[\left[\left(m_{cem} + m_{FA}\right) - m_{clink}^{ult}\right]\frac{\left(\Gamma_{ult} - \Gamma_{endST1}\right)}{\Gamma_{ult}} + m_{clink}^{ult}\right] \tag{21}$$

Our somewhat phenomenological approach to the simulation of self-healing transport and precipitation processes warrants a few further remarks. A number of authors have recently developed models that attempt to simulate the diffusion of individual ions and precipitation of specific chemicals (e.g. calcite) [46–48]. These models are dependent and sensitive to some highly variable and uncertain parameters, such as chemical diffusion and kinetic rate constants as well as permeability coefficients. This type of model would become very

expensive if all of the chemical processes associated with self-healing cementitious materials were to be simulated. Indeed, if models are going to be employed for the analysis of real structures, some more tractable and efficient approaches are needed in the near to mid-term. The proposed semi-phenomenological model potentially provides such an approach. As Hilloudin et al. [18] point out '*Modelling the autogenous healing in concrete is still a great challenge because it relies on the development of coupled models. Further investigations are needed to understand the recovery of mechanical and transport properties'*.

Most authors agree that 'autogenic' self-healing is greatest in young cementitious materials when there is a significant amount of unhydrated cement and water [3,11,12,16,47]. By implication, under these conditions, materials have a more open pore structure than in their mature state. The pore structure, in particular the network of capillary pores, is known to be a significant factor in the efficiency of self-healing [47]. The proposed model is able to capture these features, particularly because it tracks the amount of hydrated material and water forms, as well as having a proper link to developing porosity. The model is most applicable to simulating self-healing in relatively young materials and since cracks frequently form in the first few months of a structure's life [49], this aspect of self-healing is considered to be very important.

A number of recent self-healing experiments have suggested that the material deposited in cracks contains significantly more portlandite (CH) (which will subsequently will form calcite in the presence of CO_2) than $C-S-H$ [16,50,51]. The hydration model considers all main hydration compounds, which encompasses both $C-S-H$ and CH, and keeps track of the amount of all main unhydrated cementitious components. Whilst the exact nature of the healing material may be of interest, the present self-healing transport model – that does not distinguish between these two main compounds – has considerable value provided the mechanical properties of the deposited material are known. These can be established from separate mechanical experiments.

The authors fully acknowledge that this model, as with all other existing coupled models for transport processes in cementitious materials, has a number of parameters that have to be calibrated for specific problems. These include the d_{cz} parameter from equation (16) and the Freundlich constants in equation (17), all of which are guided by general considerations and previous work and then calibrated using the examples below. As with other existing coupled models for cementitious materials, true predictions can only be undertaken if sufficient prior data exists for calibration.

4. Numerical formulation

The non-linear system, which comprises equations (4) to (6), is solved in space by means of the finite element method formulated using Galerkin's weighting procedure [19,20,52]. The equilibrium relationships are expressed in terms of the principal variables S_w^{cap}, T and ω in the domain Ω and Cauchy type boundary conditions from equations (22), (23) and (24) are applied.

$$\left(J_w^A + J_v^D\right)\cdot\overline{n} - q_{wv} - \delta_{wv}\left(\rho_v - \rho_v^{env}\right) = 0 \qquad \text{on } \Gamma_{q1} \tag{22}$$

$$\left(J_T^{CD} - J_w^A \Delta H_v\right)\cdot\overline{n} - q_T - \delta_T\left(T - T^{env}\right) = 0 \qquad \text{on } \Gamma_{q2} \tag{23}$$

$$\left(J_\omega^A + J_\omega^{DD}\right)\cdot\overline{n} - q_\omega - \delta_\omega\left(\omega - \omega^{env}\right) = 0 \qquad \text{on } \Gamma_{q3};\ \ \Gamma_q = \Gamma_{q1}\cup\Gamma_{q2}\cup\Gamma_{q3} \tag{24}$$

The Gauss-Green Divergence Theorem [19] is used to obtain the weak form of the elemental system of equations, which is then assembled to give the following global algebraic system:

$$\begin{bmatrix} \hat{\boldsymbol{C}}_{11} & \hat{\boldsymbol{C}}_{12} & \hat{\boldsymbol{C}}_{13} \\ \hat{\boldsymbol{C}}_{21} & \hat{\boldsymbol{C}}_{22} & \hat{\boldsymbol{C}}_{23} \\ \hat{\boldsymbol{C}}_{31} & \hat{\boldsymbol{C}}_{32} & \hat{\boldsymbol{C}}_{33} \end{bmatrix} \begin{Bmatrix} \dot{\boldsymbol{S}}_{\boldsymbol{w}}^{\boldsymbol{cap}} \\ \dot{\boldsymbol{T}} \\ \dot{\boldsymbol{\omega}} \end{Bmatrix} + \begin{bmatrix} \hat{\boldsymbol{K}}_{11} & \hat{\boldsymbol{K}}_{12} & \hat{\boldsymbol{K}}_{13} \\ \hat{\boldsymbol{K}}_{21} & \hat{\boldsymbol{K}}_{22} & \hat{\boldsymbol{K}}_{23} \\ \hat{\boldsymbol{K}}_{31} & \hat{\boldsymbol{K}}_{32} & \hat{\boldsymbol{K}}_{33} \end{bmatrix} \begin{Bmatrix} \boldsymbol{S}_{\boldsymbol{w}}^{\boldsymbol{cap}} \\ \boldsymbol{T} \\ \boldsymbol{\omega} \end{Bmatrix} = \begin{Bmatrix} \hat{\boldsymbol{F}}_1 \\ \hat{\boldsymbol{F}}_2 \\ \hat{\boldsymbol{F}}_3 \end{Bmatrix} \tag{25}$$

$$\hat{\boldsymbol{C}}_{ij} = \sum_{e=1}^{ne} \int_{\Omega^e} \boldsymbol{N} C_{ij} \boldsymbol{N}^T d\Omega^e \tag{26}$$

$$\hat{\boldsymbol{K}}_{ij} = \sum_{e=1}^{ne} \int_{\Omega^e} \boldsymbol{N} K_{ij} \boldsymbol{N}^T d\Omega^e \tag{27}$$

$$\hat{\boldsymbol{F}}_i = \sum_{e=1}^{ne} \left(\int_{\Omega^e} \nabla \boldsymbol{N} f_{gi} d\Omega^e + \int_{\Gamma_{qi}^e} \boldsymbol{N} F_{qi} d\Gamma_{qi}^e + \int_{\Omega^e} \boldsymbol{N} F_{\Gamma i} d\Omega^e \right) \tag{28}$$

The integrands included in the assembling procedure depend on the principal variables as can be seen in Annex C. Further details may be found in [21].

To perform the time discretisation of the proposed THC model, an implicit finite difference approximation [19] is applied to equation (29) that represents the condensed form of matrix equation (25):

$$\hat{\boldsymbol{C}}\dot{\boldsymbol{\Phi}} + \hat{\boldsymbol{K}}\boldsymbol{\Phi} = \hat{\boldsymbol{F}} \tag{29}$$

The residual of the above relationship at the current time step n equals:

$$\boldsymbol{\Psi}(\boldsymbol{\Phi_n}) = \hat{\boldsymbol{C}}(\boldsymbol{\Phi_n} - \boldsymbol{\Phi_{n\text{-}1}}) + (t_n - t_{n-1})\left(\hat{\boldsymbol{K}}\boldsymbol{\Phi} - \hat{\boldsymbol{F}}\right) \tag{30}$$

This residual is minimised for each time step in a Newton-Raphson-type iterative procedure. The vector of variables is updated successively by the increment $\delta\boldsymbol{\Phi}_n^{k+1}$ until the L2 norm of $\boldsymbol{\Psi}$ is lower than a specified tolerance:

$$\boldsymbol{\Phi}_n^{k+1} = \boldsymbol{\Phi}_n^k + \delta\boldsymbol{\Phi}_n^{k+1} \tag{31}$$

The increment is computed using the standard procedure of equating the truncated form of Taylor's series expansion for $\boldsymbol{\Psi}$ to zero, which results in the following:

$$\delta\boldsymbol{\Phi}_n^{k+1} = \begin{bmatrix} \frac{\partial\boldsymbol{\Psi}_1\left(\boldsymbol{\Phi}_n^k\right)}{\partial\boldsymbol{\Phi}_1} & \frac{\partial\boldsymbol{\Psi}_1\left(\boldsymbol{\Phi}_n^k\right)}{\partial\boldsymbol{\Phi}_2} & \frac{\partial\boldsymbol{\Psi}_1\left(\boldsymbol{\Phi}_n^k\right)}{\partial\boldsymbol{\Phi}_3} \\ \frac{\partial\boldsymbol{\Psi}_2\left(\boldsymbol{\Phi}_n^k\right)}{\partial\boldsymbol{\Phi}_1} & \frac{\partial\boldsymbol{\Psi}_2\left(\boldsymbol{\Phi}_n^k\right)}{\partial\boldsymbol{\Phi}_2} & \frac{\partial\boldsymbol{\Psi}_2\left(\boldsymbol{\Phi}_n^k\right)}{\partial\boldsymbol{\Phi}_3} \\ \frac{\partial\boldsymbol{\Psi}_3\left(\boldsymbol{\Phi}_n^k\right)}{\partial\boldsymbol{\Phi}_1} & \frac{\partial\boldsymbol{\Psi}_3\left(\boldsymbol{\Phi}_n^k\right)}{\partial\boldsymbol{\Phi}_2} & \frac{\partial\boldsymbol{\Psi}_3\left(\boldsymbol{\Phi}_n^k\right)}{\partial\boldsymbol{\Phi}_3} \end{bmatrix}^{-1} \begin{bmatrix} -\boldsymbol{\Psi}_1\left(\boldsymbol{\Phi}_n^k\right) \\ -\boldsymbol{\Psi}_2\left(\boldsymbol{\Phi}_n^k\right) \\ -\boldsymbol{\Psi}_3\left(\boldsymbol{\Phi}_n^k\right) \end{bmatrix} \tag{32}$$

where the Jacobian of the approximation error, $\frac{\partial\boldsymbol{\Psi}}{\partial\boldsymbol{\Phi}}$, is:

$$\frac{\partial\boldsymbol{\Psi}_p}{\partial\boldsymbol{\Phi}_r} = \left\{\hat{\boldsymbol{C}}_{pr} + \sum_{t=1}^{nn}\sum_{s=1}^{3}\frac{\partial\hat{\boldsymbol{C}}^t_{ps}}{\partial\boldsymbol{\Phi}_r}\Delta\Phi_{s_t}\right\} + \left(t_n - t_{n-1}\right)\left\{\hat{\boldsymbol{K}}_{pr} + \sum_{t=1}^{nn}\sum_{s=1}^{3}\frac{\partial\hat{\boldsymbol{K}}^t_{ps}}{\partial\boldsymbol{\Phi}_r}\Phi_{s_t}\right\} \tag{33}$$

$p, r \in [1,3]$; nn = number of nodes per finite element

$\Delta\Phi_{s_t}$ = difference between the current and the previous value of Φ_{s_t}

5. Numerical simulations

In the following section, three self-healing experiments are considered. The first is based on data obtained by Davies [53] in our laboratories at Cardiff, the other two use data from the tests of Huang et al. [16] and Van Tittelboom [50] respectively. The selection of the experiments was made with the intention of testing the efficiency of the proposed THC model under different healing conditions. Attention was focused on studying the influence of the crack width and of the available quantity of unhydrated cement upon the material behaviour. The mix designs listed in Table 1, which are made of Portland cements with different chemical compositions (see Table 2), were investigated. Their porous network and hydration characteristics were evaluated numerically using the microstructural model STOICH_HC2 in order to provide the input needed for the autogenous healing model. The parameters given by STOICH_HC2, required for defining the porosity curves and the initial concentration of unreacted clinker in the capillary water, are found in Table 3.

Table 1 Mix design of investigated cementitious materials

Mix type	m_{cem}	m_{FA}	m_w	m_{agg}	V_{ea}	ρ_{cem}	ρ_{FA}	ρ_{agg}	ρ_{dry}
M1	400	171.4	285.7	1200	0.015	3168	2330	2400	1770

M2	1614	–	484.2	–	0.003	3150	–	–	1615
M3	539	–	215.6	1617	0.003	3150	–	2650	2156

303

304

305

306

Table 2 Chemical composition of different types of cementitious mixes

307

	cement type	f_{C_3A}	f_{C_3S}	f_{C_2S}	f_{C_4AF}	f_{SO_3}	f_{gypsum}	
M1	CEM II/B-V 32.5R	3.03	57.28	23.98	7.59	2.04	4.39	
M2	CEM 42.5N	8.00	64.00	13.00	9.00	2.57	5.53	[16]
M3	CEM I 52.5 N	6.34	63.88	5.50	12.14	3.07	6.60	[54]

308

Table 3 Data from STOICH_HC2 model

309

	$C_{\eta S}^{cap}$	$C_{\eta S}^{tot}$	m_{CW}^{ult}	m_{LGW}^{ult}	m_{clink}^{ult}	Γ_{ult}
M1	0.279	0.144	121.77	29.92	17.76	1
M2	0.204	0.104	0.13	89.85	515.58	0.67
M3	0.272	0.138	≈0	39.91	38.29	0.98

310

311 As was discussed earlier, in the crack region there is an increased water-cement ratio and
312 thus a greater porosity of the deposited material is expected. In order to estimate d_{cz} from
313 equation (16), a local w/c ranging between 4.5 and 5 was assumed. Thus, the adopted
314 values of d_{cz} are: 3.2 for M1, 3.4 for M2 and 5.5 for M3.

315 Regarding the reactive transport processes associated with self-healing, Table 4 provides
316 the data necessary for defining the movement of the solute and the Freudlich type isotherm
317 mentioned in equation (17). In this table the reader can also identify the values of the
318 thermo-hygral material parameters that vary with the mix composition. In all of the examples,
319 the density of the precipitated material, ρ_P, is taken 2600 kg/m^3, whilst the tolerance used in
320 the Newton-Raphson solution of the nonlinear finite element equations is taken as 10^{-3}.
321 Table 4 also includes some additional comments that provide guidance of how these model
322 parameters were obtained.

323

Table 4 Thermo-hygro-chemical parameters

	M1	M2			M3	Comments
		7 days	14 days	28 days		
α_P	2.5	0.042	0.023	0.025	5.5	α_P and β_P are guided by general considerations found in [42,55] and then calibrated using the examples below.
β_P	0.07	10	10	8	1	
C_p^s / C_p^{FA}	840	840			840	C_p^s / C_p^{FA} is based on the value given in reference [56].
D_{mol}	$1*10^{-8}$	$3*10^{-9}$			$5*10^{-8}$	D_{mol} were originally set to the values $1*10^{-9}$ m^2/s and $1.44/1.62/1.82*10^{-9}$ m^2/s given in [42] and [57], respectively, and then calibrated for the present data.
δ_{wv}	$2.5*10^{-4}$	$3*10^{-4}$			$3*10^{-3}$	δ_{wv} and δ_T are based on the values given in reference [22].
δ_T	4	13			4	
δ_ω	10^{-6}	10^{-6}			10^{-6}	δ_ω is based on the value given in reference [57].
$k_w^{\text{int}mat}$	$5*10^{-21}$	$2*10^{-21}$			$2*10^{-21}$	$k_w^{\text{int}mat}$ were originally set to the values $5*10^{-21}$ m^2 and $6*10^{-22}$ m^2 given in [22] for cement pastes and concrete mixes and then calibrated for the present data. Their values are also similar those reported in [58].
a	183.80	370.57			183.80	a, b and $c\eta$ are based on the values given in reference [22] for cement pastes and concrete mixes.
b	2.28	2.17			2.28	
$c\eta$	-10	-11			-10	

5.1 Example 1

In the first experiment considered [53], a rectangular beam (255 X 75 X 75mm) was cast using the cementitious mix M1. A steel shim was used to pre-form a narrow central notch of 0.2mm in the lower face of the specimen, as can be seen in Figure 3 (a). The beam was left in the mould and covered with a hessian sack for 26 hours at 50% environmental relative humidity and 293K. The steel shim was removed after the first 6 hours and the mortar beam was completely immersed in water for 13, 27 and 41 days. At the end of these time intervals,

334 the sample was broken in a three-point bending test and the crack recovery was visually
335 measured at the central notch. The camera images of the cross section revealed the
336 formation of a white crystalline substance on the external surface and the building up of a
337 ridge of material with the same colour as the bulk sample, in the interior. SEM tests detected
338 portlandite (CH), ettringite ($C_6A\bar{S}_3H_{32}$) and calcium-silicate-hydrate, whilst XRD tests
339 identified portlandite, silica and calcite ($CaCO_3$) in the composition of the deposited material.
340 All the images were processes using ImageJ (see Figure 2) and the degree of self-healing in
341 terms of area fraction of new precipitated material was estimated.
342

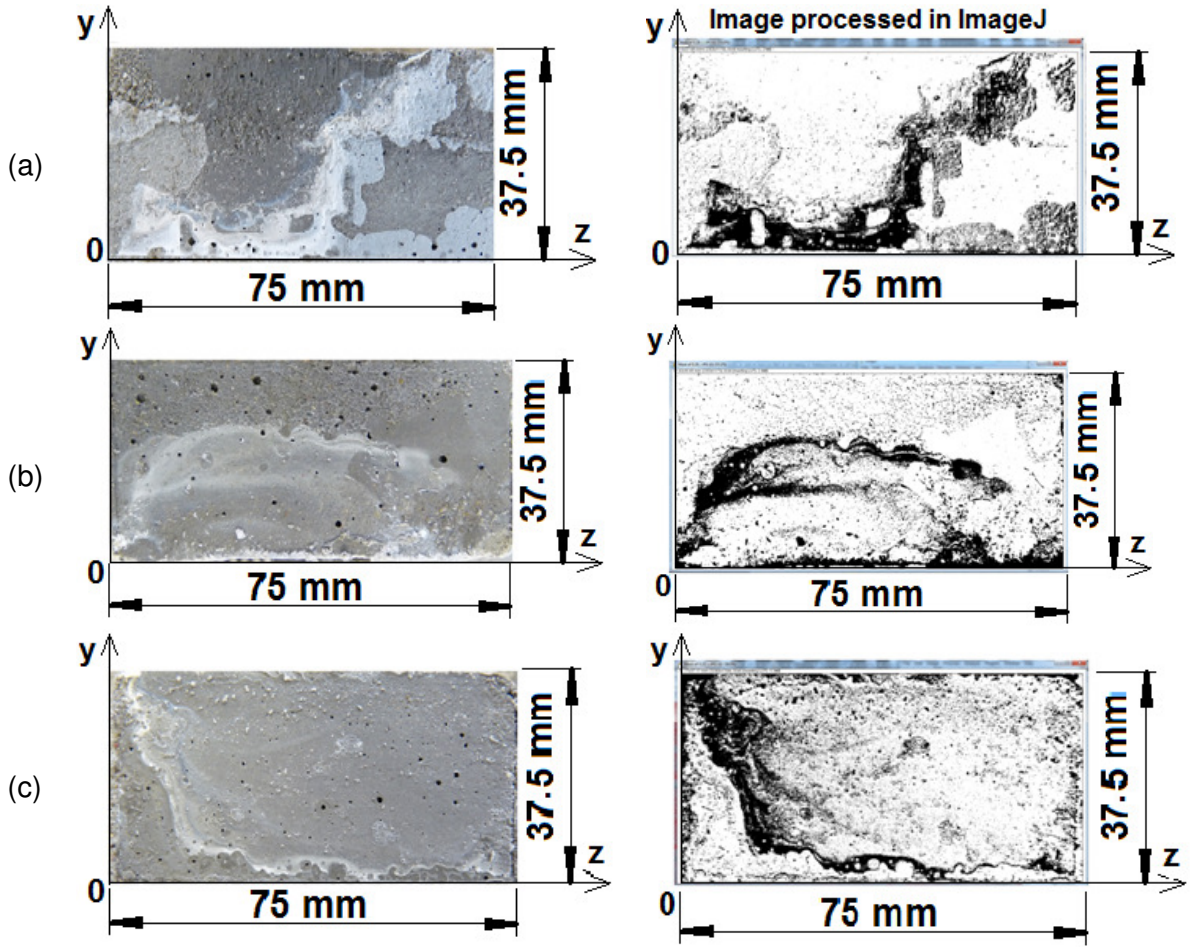

Figure 2 Samples of processed self-healed cross sections at (a) 13, (b) 27 and (c) 41 days; h_x = 127.4 mm

The environmental conditions were symmetrical with respect to the middle cross section throughout the self-healing process. The proportion of mesh adjacent to the crack, which is formed of 101 (21 X 5) bilinear finite elements, is depicted Figure 3 (b).

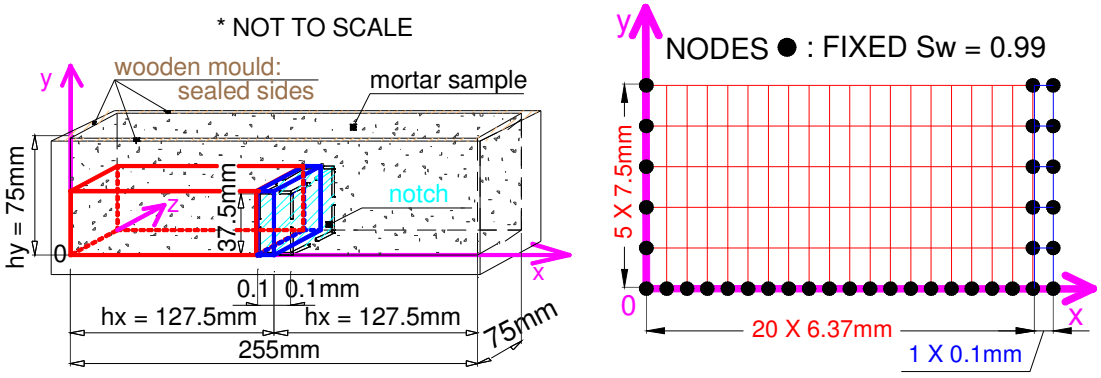

Figure 3 Experimental set-up of the example 1

For the time discretisation, a varying time step Δt , expressed in seconds, is adopted:

$$\Delta t = \begin{cases} 3600, & 1 \le itime \le 200 \\ 7200, & 200 < itime \le 250 \\ 10800, & 250 < itime \le 300 \\ 14400, & 300 < itime \end{cases} \tag{34}$$

The thermo-hygral variables at the beginning of the self-healing process correspond to the values reached at 26 hours after casting. A preliminary TH simulation of the moist air curing (using the model in [22]) stage was carried out to evaluate the TH state at the end of this stage, the results from which are presented in Figure 4. The corresponding hydration degree of the mix, used in equations (21) and **Error! Reference source not found.**, equals to Γ_{endST1} = 0.30, while the initial concentration of solute is ω_0 = 0.49.

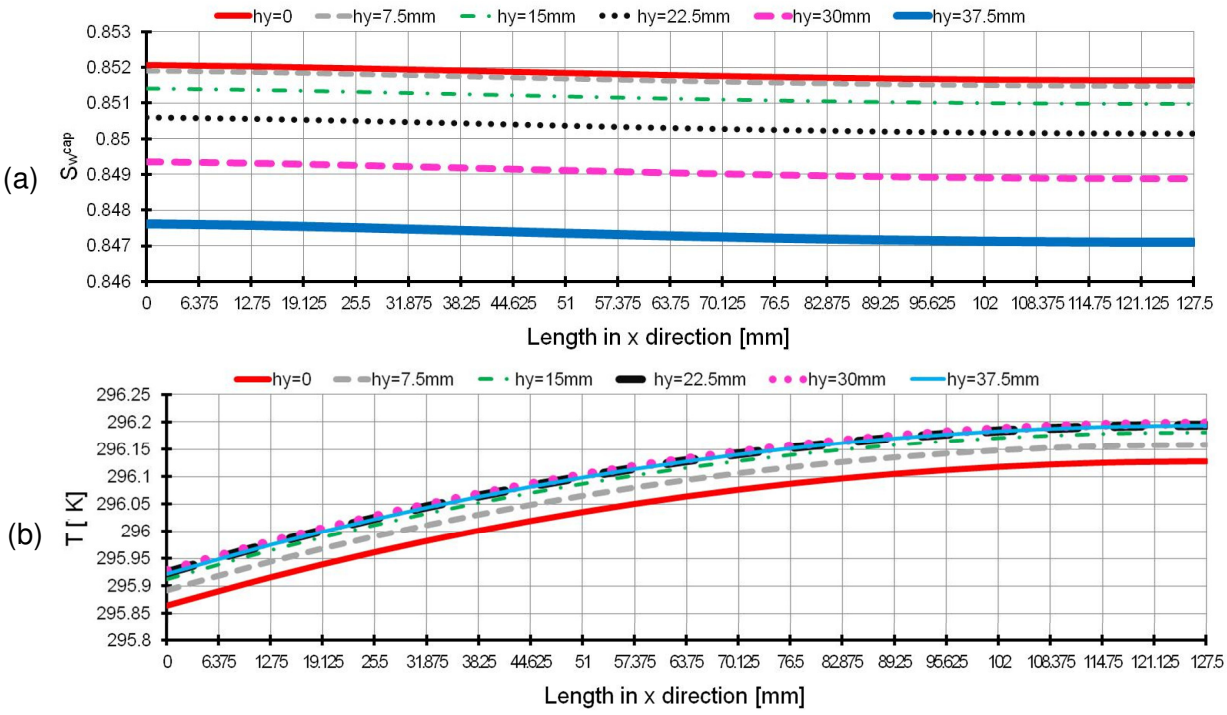

Figure 4 Example 1: distribution of S_w^{cap} and T at the end of moist air curing

The Freundlich type isotherm is calibrated to account for both the potential ongoing hydration and carbonation. The numerical results from Figure 5 show that the deposition of the new material occurs during the first days of autogenous healing throughout the sample.

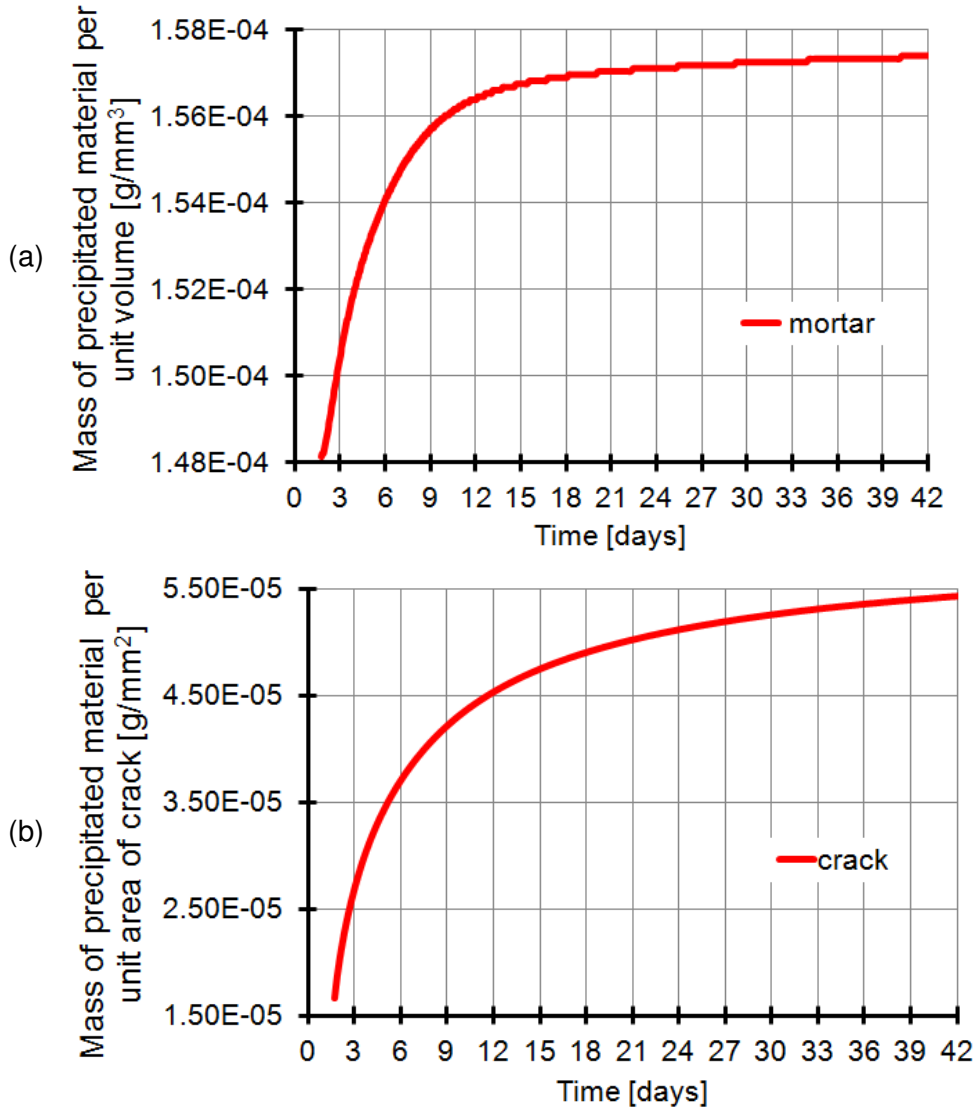

364

Figure 5 Distribution in time of the mass of precipitated material in (a) mortar and (b) crack

365

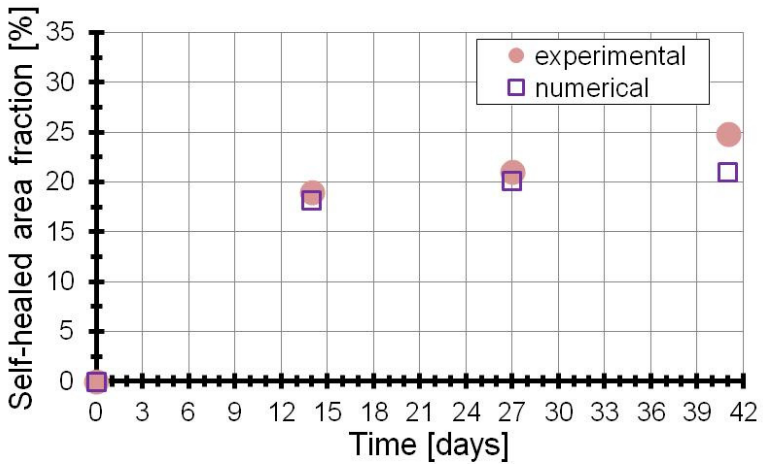

366

Figure 6 Evolution of the self-healed area fraction in the crack

However, the process is less intense within the mortar beam and diminishes after the 3rd day, while in the crack region, the accumulation is continuous and much more significant. In terms of self-healed area fraction, Figure 6 confirms that the numerical findings are in good agreement with the experimental data, especially at the 14th and 27th day of curing.

5.2 Example 2

The second example simulates the experiment performed by Huang et al. [16] that quantifies, by means of ESEM observations, the precipitation of healing products in cracks having w_{ref} ≈ 10μm in width. The cement paste prisms M2 (160 X 40 X 40mm) were cast and subjected to controlled three-point bending tests after 7, 14 and 28 days from casting. Once the crack was formed, the specimens were introduced in sealed containers partially filled with water, in order to avoid carbonation, and left there to heal for about 200 hours. The temperature measured in the surrounding environment of the prisms was 20 ± 1℃. The schematic representation of the experiment is given in Figure 7 (a).

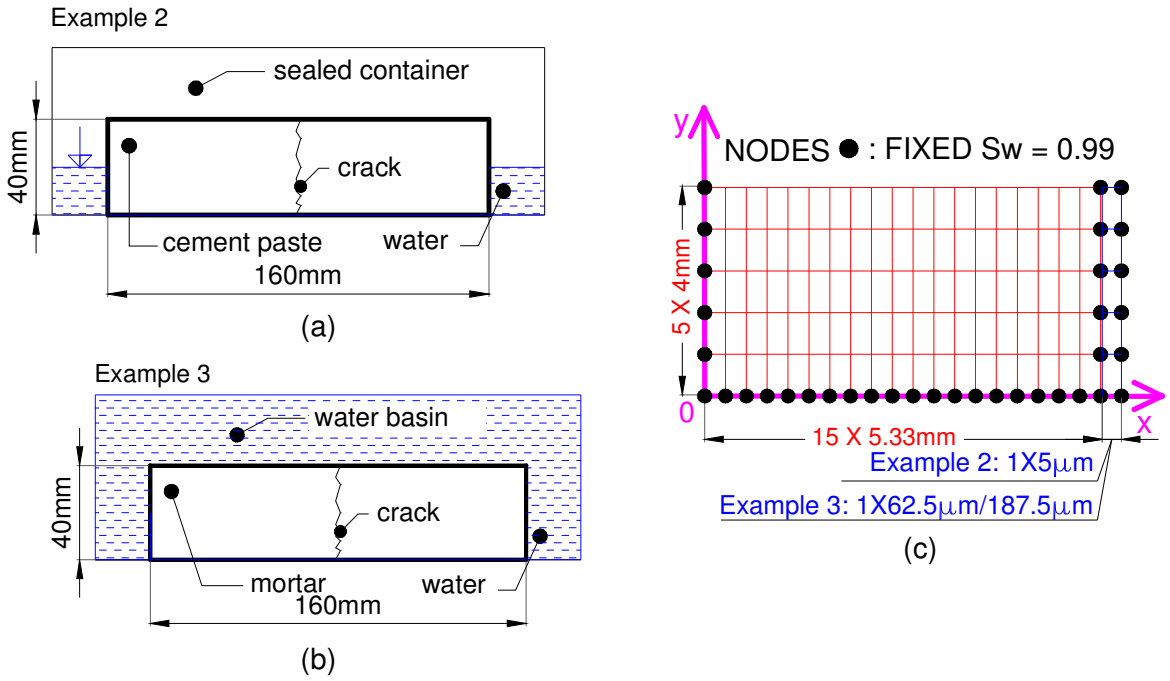

Figure 7 Experimental set-up and meshing for the numerical examples 2 and 3

The present model does not consider capillary flow in the discrete crack, in the sense described by Gardner et al. [59]. However, our continuum flow model predicts that the entire crack becomes saturated during the self-healing period, which is consistent with the experimental observations of Huang et al. [16].

At the end of the self-healing period, the morphology of the precipitates was investigated using ESEM equipped with EDS, whilst the mineralogy and the percentage of each constituent in the crack were established in FTIR and TGA tests. Huang et al. identified both crystal and gel-like healing products that contained: CH, $CaCO_3$ and other hydrates, including $C-S-H$.

The amount of newly formed hydrates was quantified using BSE image analysis. The specimens were impregnated with epoxy, cut in 3 sections along the crack and 105 images per specimen were taken and examined. The effective measured crack width at different times was employed to compute the normalized filling fraction according to:

$$\gamma_{norm} = \gamma \cdot \frac{w_{crack}}{w_{ref}} \tag{35}$$

During the self-healing experiment, only the bottom part of the prism was submerged due to a limited amount of water. Moreover, the environmental conditions were symmetrical with respect to the middle cross section. The proportion of mesh adjacent to the crack, composed of 80 (16 X 5) bilinear finite elements, is depicted in Figure 7 (c).

For this numerical example a constant time step equal to 3600 seconds was chosen. The starting values of S_w^{cap} and T, presented here in Figure 8, as well as the initial hydration degrees and concentrations of solute, listed in Table 5, were taken from a TH simulation (using the model in [22]) that considered moisture sealed curing conditions for 7, 14 and 28 days. The modelled crack had an initial size of 10μm and was filled with water throughout the experiment.

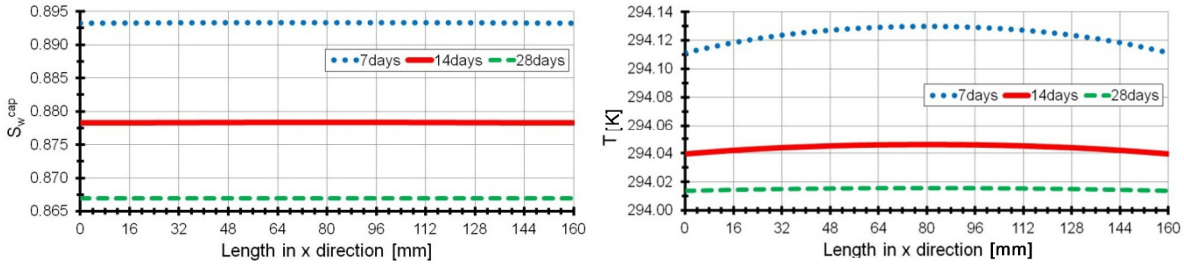

Figure 8 Example 2: distribution of S_w^{cap} and T before autogenous healing

Table 5 Initial values for Example 2

	7 days	14 days	28 days
Γ_{endST1}	0.54	0.58	0.62
ω_0	1.30	1.39	1.47

Figure 9 shows the self-healing efficiency due to further hydration under saturated conditions. The simulation results are reasonably consistent with the experimental findings, especially for the first 150 hours in the case of the specimen cracked at 7 days. In the case of the older cement pastes, that are plotted in Figure 9 (b) and (c), a slight overestimation of the crack recovery can be observed. Nevertheless, as can be seen in Figure 9 (d), the proposed THC model confirms the experimental observation that the filling fraction of the crack diminishes with the maturity of the paste.

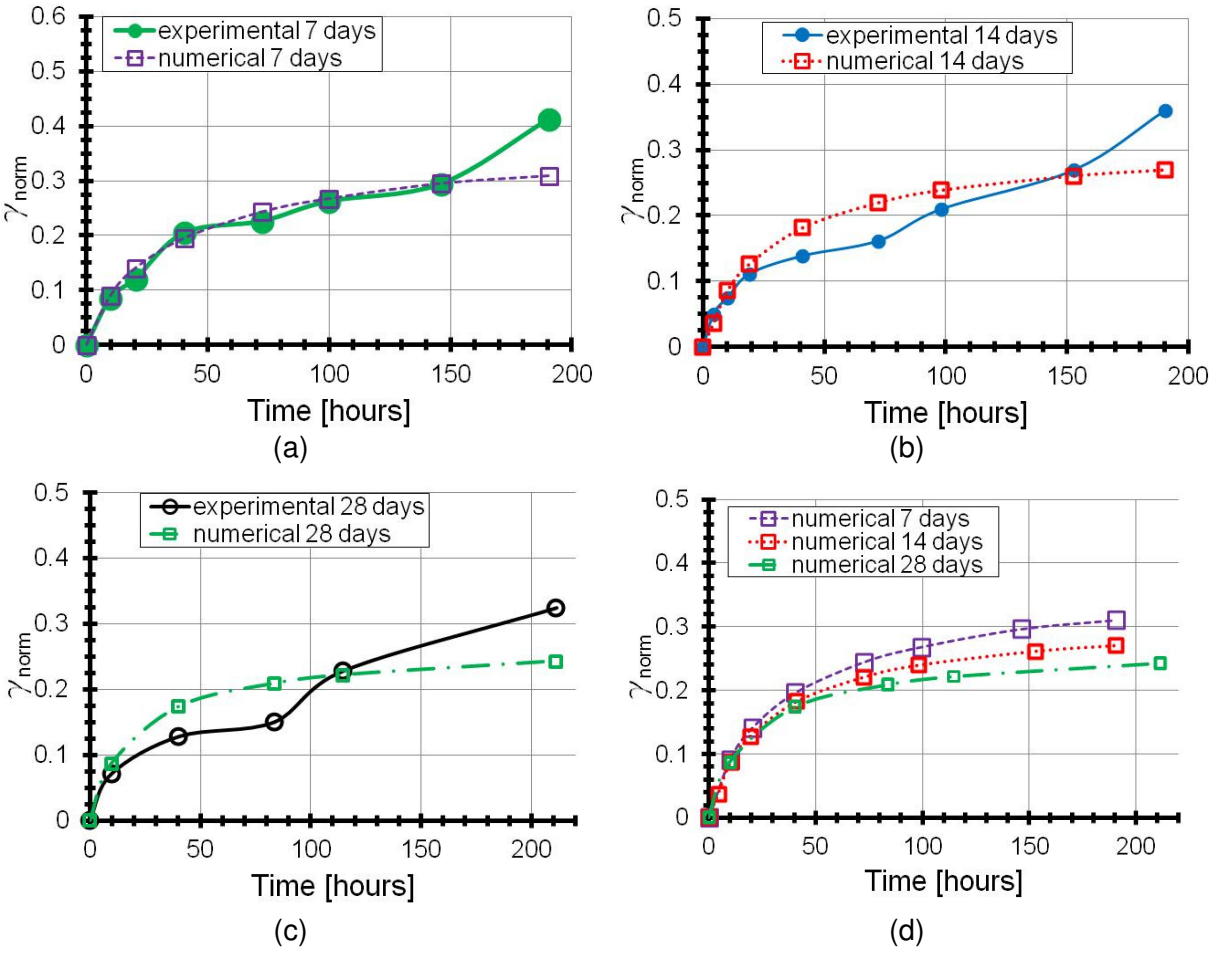

Figure 9 Example 2: Normalized filling fractions

5.3 Example 3

The experiments considered in this third example [50] used reinforced mortar prisms (mix designation M3, dimensions 160 X 40 X 40mm and two 2mm diameter reinforcing bars), which were cast and left in an air conditioned room (20 ± 1°C and relative humidity > 95%). At 28 days the specimens were first subjected to cracking in a three-point bend test and then were totally immersed in basins filled with tap water for 1, 4, 7, 21 and 42 days, as illustrated in Figure 7 (b). When removed from the basins, the surfaces of the specimens were dried

with paper towels and exposed to the air for a few minutes. The change in crack width at the surface of each specimen was measured in nine locations using a stereo microscope equipped with a camera. The visual investigation at the crack surface revealed the formation of a white crystalline material reported to be $CaCO_3$ [50]. The measured surface crack widths were plotted as a function of the initial surface crack width and two areas, $A_{crack}(t_0)$ and $A_{crack}(t)$, were computed. The first represents the area under the curve connecting the initial measuring points, while the second corresponds to the area under the curve connecting the measuring points obtained after t days of water immersion. The crack self-healing ratio ($\gamma(t)$) for cracks ranging between 0 - 125μm and 125 - 250μm was defined by Van Tittelboom, et al. [50] to be:

$$\gamma(t) = 1 - \frac{A_{crack}(t)}{A_{crack}(t_0)} \tag{36}$$

The spatial discretisation in the vicinity of the crack is composed of 80 (16 X 5) bilinear finite elements as can be seen in Figure 7 (c). The crack widths considered are the mean values of the above mentioned ranges, that is 62.5μm and 187.5μm. Figure 10 provides the initial values of the TH variables considered.

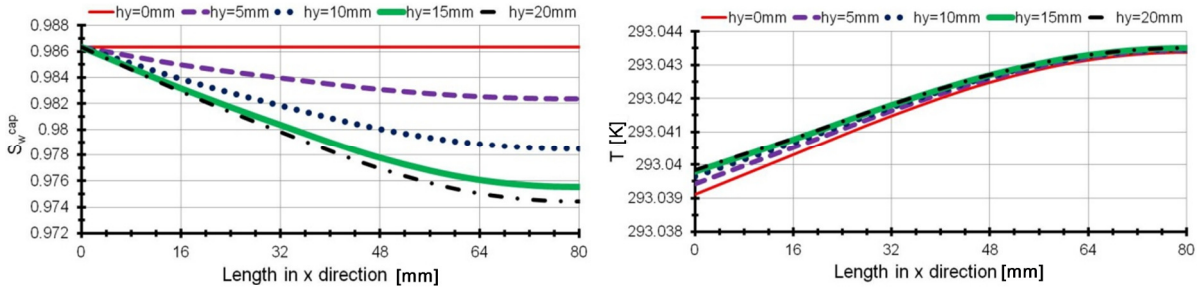

Figure 10 Example 3: distribution of S_w and T before self-healing

The microstructural model STOICH_HC2 shows that 91% of the hydration reaction had occurred before the onset of self-healing and that 38.29 kg/m^3 of unreacted clinker can still be found in the mix. Hence, for these experimental conditions, ω_0 is equal to 0.43. The time step selected for the Newton-Raphson procedure is the same used for numerical example 1.

The comparison of the current simulations with the experimental data is illustrated in Figure 11. The numerical results in the case of the 62.5μm crack closely match the laboratory data reported by Van Tittelboom et al. [50]. It is evident that in less than 14 days of curing, the precipitates have filled more than 95% of the crack. For the larger crack however, the healing capacity is visibly over estimated for day 3 (of curing) and underestimated for the 42nd day. In this case, the recovery reaches only approximately 70%.

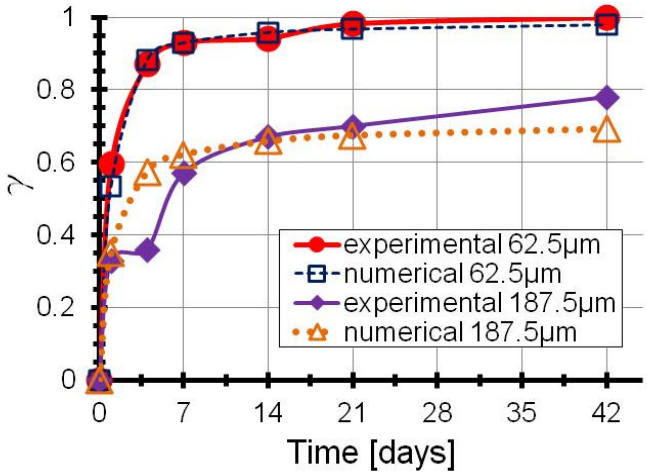

Figure 11 Example 3: Evolution of the crack self-healing ratio

The amount of material transported is sensitive to both the diffusion and advection model parameters, and thus we conclude that it is important to consider both mechanisms in such a model. In all three examples we have simulated self-healing from the amount of unhydrated cement in suspension at the start of the healing period. It has been assumed that the solid deposited in the cracks derives from the cement employed in the experiments simulated, although the individual nature of the compounds deposited is not distinguished in these simulations. Knowledge of the rate of crack filling is one of the essential components needed for a prediction of the coupled thermo-hygro-chemico-mechanical (THCM) response of an autogenous self-healing system. In addition, the mechanical properties of the deposited hydrated-cement, along with the bond properties of interface between the matrix and crack-filling material, are also required. These have not been obtained here but it is believed that the present model shows that a semi-phenomenological model, that considers dissolved clinker as a single reactive transport variable, can adequately represent some of the important aspects of a self-healing system.

6. Conclusions and closing remarks

In this paper a coupled thermo-hygro-chemical model was described for the simulation of autogenous healing in ordinary cementitious materials. Further hydration was modelled and a general reactive transport process was simulated in which the solute consisted of the four main clinker minerals. The proposed model traced in time the concentration of the dissolved material from the unhydrated cement. An equilibrium Freundlich type isotherm was chosen to enable the phase change and therefore the formation of the healing products in the cracks. The following conclusions can be drawn from the work:

- the model is most applicable to self-healing in relatively young cementitious materials;
- diffusion and advection both have a significant influence on the amount of material transported to a crack during early age self-healing;
- the porosity of the precipitate in the crack region is higher than the porosity of the hydrates found in the bulk material;
- the calculated filling fraction of cracks is in agreement with the quantitative results reported in the literature, which signifies that the proposed THC model behaves satisfactory when predicting autogenous healing;
- larger amounts of unhydrated cement leads to higher filling fractions, although the initial concentration of the solute in younger cement pastes is lower;
- the degree of autogenous crack healing increases with reducing crack width.

The requirement for model parameters to be calibrated to experimental data is a feature of this and other THC models. The issue of defining easily identifiable model parameters, determining their values and statistical characteristics, and reliably establishing the sensitivity of model simulations to these parameter values are some of the major challenges facing researchers on THCM models for self-healing materials.

7. Acknowledgements

We gratefully acknowledge support from LUSAS - developer and supplier of Finite Element Analysis (FEA) application software products - and also acknowledge the cooperation from the team working on the EPSRC M4L project for the provision of experimental data used for the model validation.

Annex A

Table A. 1 Chemical reactions for the hydration of ordinary Portland cements

	Stage	Stoichiometry of the reaction	Ref.
C_3A	I	$C_3A + 3C\bar{S}H_2 + (z_1 - 6)H \rightarrow C_6A\bar{S}_3H_{z_1}$	[44,60]
	II	$C_3A + C_6A\bar{S}_3H_{z_1} + (3z_2 - z_1)H \rightarrow 3C_4A\bar{S}H_{z_2}$	[44,60]
	III	$C_3A + C_4A\bar{S}H_{z_2} + CH + (2z_3 - z_2)H \rightarrow 2C_3A(C\bar{S}, CH)H_{z_3}$	[61]
		$C_3A + CH + (z_4 - 1)H \rightarrow C_4AH_{z_4}$	[44]
C_3S	I	$C_3S + (1.3 + y)H \rightarrow C_{1.7}SH_y + 1.3CH$	[62]
C_2S	I	$C_2S + (0.3 + y)H \rightarrow C_{1.7}SH_y + 0.3CH$	[62]
C_4AF	I	$0.75C_4AF + 3C\bar{S}H_2 + (z_5 + 0.5z_6 - 6)H \rightarrow C_6(A,F)\bar{S}_3H_{z_5} + 0.5(F,A)_{z_6}$	[44,61]
	II	$1.5C_4AF + C_6(A,F)\bar{S}_3H_{z_5} + (3z_7 + z_6 - z_5)H \rightarrow 3C_4(A,F)\bar{S}H_{z_7} + (F,A)_{z_6}$	[44,61]
	III	$C_4AF + 2CH + (2z_8 - 2)H \rightarrow 2C_3(A,F)H_{z_8}$	[63]

Table A. 2 Stoichiometric coefficients for the hydration reactions of Portland cement

Relative humidity	y	z_1	z_2	z_3	z_4	z_5	z_6	z_7	z_8
[60%,40%)	4	32	12	12	13	32	3	12	6
[40%,11%)	3.15	25.06	10.89	9.75	10.56	26	2.43	9.75	4.88
[11%,0%)	2.10	14.41	9.19	6.30	6.83	16.80	1.58	6.30	3.15
≈0%	1.30	7	8	4.40	4.23	10.40	0.98	3.90	1.95

Table A. 3 Kinetic parameters of cement mixes taken from [64] according to [30]

Kinetic parameter	w/c	C_3S	C_2S	C_3A	C_4AF
Γ_X^I		0.02	$1*10^{-6}$	0.04	0.4
t_X^I	0.5	856.8	0.2	7084.8	30816
	0.4	914.4	0.2	7696.8	34848
	0.3	972	0.3	8308.8	38880
κ_X	0.5	0.05	0.02	0.02	0.02
	0.4	0.04	0.01	0.02	0.02
	0.3	0.04	0.01	0.02	0.02
K_X	0.5	1.72	0.96	1.00	2.30
	0.4	1.79	1.03	1.07	2.37
	0.3	1.86	1.10	1.14	2.44
t_X^{NG}	0.5	$3.66*10^4$	$4.67*10^4$	$3.59*10^4$	$7.95*10^4$
	0.4	$4.17*10^4$	$6.02*10^4$	$4.54*10^4$	$9.38*10^4$
	0.3	$4.72*10^4$	$7.58*10^4$	$5.64*10^4$	$1.09*10^4$
D_X		$6.94*10^{-20}$	$2.22*10^{-20}$	$11.11*10^{-20}$	$2.50*10^{-20}$
Γ_X^{NG}		0.27	0.21	0.19	0.45
R_{ck}			$251*10^{-6}$		

Annex B

Table B. 1 Constitutive laws for the TH behaviour of cementitious materials

	$p_{cap} = p_g - p_w$	(B. 1)
Kelvin's law:	$RH = \frac{p_v}{p_v^{sat}} = \exp\left(-\frac{p_{cap} M_w}{\rho_w RT}\right)$ $M_w = 18,\ R = 8314.5$	(B. 2)
Dalton's law:	$\rho_g = \rho_v + \rho_{da};\ p_g = p_v + p_{da}$	(B. 3)
Antoine's law:	$p_v^{sat} = b_1 \cdot 10^{\left[b_2 - \frac{b_3}{b_4 + (T - b_5)}\right]}$ $b_1 = 133.32,\ b_3 = 1730.63,\ b_5 = 273,\ b_2 = 8.07,\ b_4 = 233.43,$	(B. 4)
Thiesen-Scheel-Diesselhorst equation [65]	$\rho_w = a_1\left[1 - \frac{(T + a_2)(T - a_3)^2}{a_4 (T + a_5)}\right]$ $a_1 = 10^3,\ a_3 = 3.99, a_5 = 68.13$ $a_2 = 288.94, a_4 = 50892.92,$	(B. 5)
Watson's formula [66]:	$\Delta H_v = \begin{cases} 2.672 \cdot 10^5 (T - T_{cr})^{0.38} & ,\forall T < T_{cr} \\ 0 & ,\forall T \geq T_{cr} \end{cases}$ $T_{cr} = 647.3$	(B. 6)
Darcy's law:	$J_w^A = \rho_w \frac{k_w^{\text{int}} k_w^{rel}}{\mu_w} grad\left(p_{cap} + \rho_w \bar{g}\right)$	
[20,35]	$k_w^{\text{int}} = k_w^{\text{int}mat} \cdot 10^{\left[A_k (T - T_{ref}) + A_\Gamma (1 - \Gamma)\right]} \left(\frac{p_g}{p_{atm}}\right)^{A_p}$ $A_k = 0.005,\ A_\Gamma = 3,$ $A_p = 1,$ $T_{ref} = 273.15$	(B. 7)
[52,67,68]	$k_w^{rel} = \sqrt{S_w^{cap}}\left[1 - \left(1 - S_w^{cap\frac{1}{m}}\right)^m\right]^2$ m from equation (B. 10)	
[35]	$\mu_w = 0.6612 \cdot (T - 229)^{-1.562}$	
Fick's law [66]:	$J_v^D = -\rho_v p_g D_v^{eff} \frac{M_w}{RT} grad\left(\frac{p_v}{p_g}\right)$ $D_v^{eff} = \eta_{cap} S_g^{A_w} f_s D_v^{ref} \left(\frac{T}{T_0}\right)^{B_v} \frac{p_{atm}}{p_g}$ $f_s = 0.001,\ A_w = 1,$ $B_v = 1.667,$ $D_v^{ref} = 2{*}10^{-5}$	(B. 8)
Fourier's law [35]:	$J_T^{CD} = -\lambda_{T_{ref}}^{eff}\left[1 + A_\lambda (T - T_{ref})\right]\left[1 + \frac{4\eta_{tot}\rho_w^{tot} S_w^{tot}}{(1 - \eta_{tot})\rho_s}\right] grad(T)$ $\lambda_{T_{ref}}^{eff} = 1.7,$ $A_\lambda = 0.0005$	(B. 9)
based on [69] and considering [70,71]::	$p_{cap} = \left[\frac{\eta_{cap}(\Gamma)}{\eta_{cap}(\Gamma_{ult})}\right]^{c\eta} a \frac{0.1171 - 0.00001516T}{0.1171 - 0.00001516T_0}\left[\left(\frac{1}{S_w^{cap}}\right)^b - 1\right]^{\frac{b-1}{b}};\quad b = \frac{1}{m}$	(B. 10)
extended Darcy's law:	$J_\omega^A = \omega J_w^A$	(B. 11)
extended linear Fick's law [43,52,72]:	$J_\omega^{DD} = -\rho_w\left(\beta_{Tr}\left\|\bar{v}^{ws}\right\|\delta_{ij} + \frac{v_i^{ws} v_j^{ws}}{\left\|\bar{v}^{ws}\right\|}(\alpha_{Lg} - \beta_{Tr}) + \eta_{cap} S_w^{cap} D_{mol}\delta_{ij}\right) grad\omega$ $\delta_{ij} = \begin{cases} 1, & i = j \\ 0, & i \neq j \end{cases};$ $\alpha_{Lg} = 5{*}10^{-3}$	(B. 12)

Annex C

Expression of the integrands used to define equations (26), (27) and (28)

$$C_{11} = \frac{\partial \overline{\rho}_w}{\partial S_w^{cap}} + \frac{\partial \overline{\rho}_v}{\partial S_w^{cap}} - \frac{\partial m_w^{des}}{\partial S_w^{cap}} \quad \text{(C. 1)}$$

$$K_{11} = -k_w \rho_w \frac{\partial p_{cap}}{\partial S_w^{cap}} + D_v^{eff} \frac{M_w}{RT} \frac{\partial p_v}{\partial S_w^{cap}} \quad \text{(C. 2)}$$

$$C_{12} = \frac{\partial \overline{\rho}_w}{\partial T} + \frac{\partial \overline{\rho}_v}{\partial T} \quad \text{(C. 3)}$$

$$K_{12} = -k_w \rho_w \left(\frac{\partial p_{cap}}{\partial T} + \frac{\partial p_{cap}}{\partial \Gamma} \frac{\partial \Gamma}{\partial T} \right) + D_v^{eff} \frac{M_w}{RT} \frac{\partial p_v}{\partial T} \quad \text{(C. 4)}$$

$$C_{13} = \frac{\partial \overline{\rho}_w}{\partial \omega} + \frac{\partial \overline{\rho}_v}{\partial \omega} \quad \text{(C. 5)}$$

$$K_{13} = 0 \quad \text{(C. 6)}$$

$$C_{21} = \left(-\frac{\partial \overline{\rho}_w}{\partial S_w^{cap}} + \frac{\partial m_w^{des}}{\partial S_w^{cap}} \right) \Delta H_v \quad \text{(C. 7)}$$

$$K_{21} = \frac{k_w^{\text{int}} k_w^{rel}}{\mu_w} \rho_w \frac{\partial p_{cap}}{\partial S_w^{cap}} \Delta H_v \quad \text{(C. 8)}$$

$$C_{22} = \overline{\rho C}_p - \frac{\partial \overline{\rho}_w}{\partial T} \Delta H_v \quad \text{(C. 9)}$$

$$K_{22} = \lambda_{T_{ref}}^{eff} \left[1 + A_\lambda \left(T - T_{ref} \right) \right] \left[1 + \frac{4 \eta_{tot} \rho_w^{tot} S_w^{tot}}{(1 - \eta_{tot}) \rho_s} \right] + \frac{k_w^{\text{int}} k_w^{rel}}{\mu_w} \rho_w \left(\frac{\partial p_{cap}}{\partial T} + \frac{\partial p_{cap}}{\partial \Gamma} \frac{\partial \Gamma}{\partial T} \right) \Delta H_v \quad \text{(C.10)}$$

$$C_{23} = 0 \quad \text{(C. 11)}$$

$$K_{23} = 0 \quad \text{(C.12)}$$

$$C_{31} = \frac{\partial \overline{\rho}_\omega}{\partial S_w^{cap}} + \alpha_P \omega^{\beta_P} \eta_{cap} \rho_w \quad \text{(C. 13)}$$

$$K_{31} = 0 \quad \text{(C.14)}$$

$$C_{32} = \frac{\partial \overline{\rho}_\omega}{\partial T} \quad \text{(C. 15)}$$

$$K_{32} = 0 \quad \text{(C.16)}$$

$$C_{33} = \frac{\partial \overline{\rho}_\omega}{\partial \omega} + \alpha_P S_w^{cap} \eta_{cap} \rho_w \beta_P \omega^{\beta_P - 1} \quad \text{(C. 17)}$$

$$K_{33} = \rho_\omega \left[\alpha_{Tr} \left| \overline{v}^{ws} \right| \delta_{ij} + \frac{v_i^{ws} v_j^{ws}}{\left| \overline{v}^{ws} \right|} \left(\alpha_{Lg} - \alpha_{Tr} \right) \right] + \rho_\omega \eta_{cap} S_w^{cap} D_{mol} \delta_{ij} \quad \text{(C.18)}$$

$$f_{g1} = \rho_w \frac{k_w^{\text{int}} k_w^{rel}}{\mu_w} \rho_w \overline{g} \quad \text{(C. 19)}$$

$$F_{q1} = q_{wv} + \delta_{wv} \left(\rho_v - \rho_v^{env} \right) \quad \text{(C.20)}$$

$$f_{g2} = -\rho_w \frac{k_w^{\text{int}} k_w^{rel}}{\mu_w} \rho_w \Delta H_v \overline{g} \quad \text{(C. 21)}$$

$$F_{q2} = q_T + \delta_T \left(T - T^{env} \right) \quad \text{(C.22)}$$

$$f_{g3} = \rho_\omega \frac{k_w^{\text{int}} k_w^{rel}}{\mu_w} \rho_w \overline{g} \quad \text{(C. 23)}$$

$$F_{q3} = q_\omega + \delta_\omega \left(\omega - \omega^{env} \right) \quad \text{(C.24)}$$

$$F_{\Gamma 1} = -\left(\frac{\partial \overline{\rho}_w}{\partial \Gamma} + \frac{\partial \overline{\rho}_v}{\partial \Gamma} + w_{tot}^{ult} \right) \dot{\Gamma} - \dot{m}_w^{agg} \quad \text{(C. 25)}$$

$$F_{\Gamma 2} = \left(\frac{\partial \overline{\rho}_w}{\partial \Gamma} + w_{tot}^{ult} \right) \Delta H_v \dot{\Gamma} + \left(Q_h + \dot{m}_w^{agg} \Delta H_v \right) \quad \text{(C. 26)}$$

$$F_{\Gamma 3} = \frac{\partial \overline{\rho}_\omega}{\partial \Gamma} + \alpha_P S_w^{cap} \omega^{\beta_P} \rho_w \frac{\partial \eta_{cap}}{\partial \Gamma} \quad \text{(C. 27)}$$

519 **References**

520 [1] L. Turner, The autogenous healing of cement and concrete: Its relation to vibrated
521 concrete and cracked concrete, in: Int. Assoc. Test. Mater., The Autoge, 1937: p.
522 pp.344.

523 [2] K. Van Tittelboom, N. De Belie, Self-Healing in cementitious materials—A review,
524 Materials (Basel). 6 (2013) 2182–2217. doi:10.3390/ma6062182.

525 [3] E. Schlangen, C. Joseph, Self-healing processes in concrete, in: S.W. Ghosh (Ed.),
526 Self-Healing Mater. Fundam. Des. Strateg. Appl., Weinheim: Wiley-VCH Verlag
527 GmbH & Co. KGaA, 2009: pp. pp.141–179. doi:10.1002/9783527625376.ch5.

528 [4] A. Neville, Autogenous healing: a concrete miracle?, Concr. Int. (2002) 76–82.

529 [5] S. Jacobsen, J. Marchand, H. Hornain, SEM observations of the microstructure of
530 frost deteriorated and self-healed concretes, Cem. Concr. Res. 25 (1995) 1781–1790.
531 doi:http://dx.doi.org/10.1016/0008-8846(95)00174-3.

532 [6] S. Granger, A. Loukili, G. Pijaudier-Cabot, G. Chanvillard, Experimental
533 characterization of the self-healing of cracks in an ultra high performance
534 cementitious material: Mechanical tests and acoustic emission analysis, Cem. Concr.
535 Res. 37 (2007) 519–527. doi:http://dx.doi.org/10.1016/j.cemconres.2006.12.005.

536 [7] N. Hearn, Self-sealing, autogenous healing and continued hydration: What is the
537 difference?, Mater. Struct. 31 (1998) 563–567. doi:10.1007/BF02481539.

538 [8] C. Edvardsen, Water permeability and autogenous healing of cracks in concrete, ACI
539 Mater. J. 96 (1999) 448–454.

540 [9] N. Hearn, C.T. Morley, Self-sealing property of concrete—Experimental evidence,
541 Mater. Struct. 30 (1997) 404–411. doi:10.1007/BF02498563.

542 [10] P. Pimienta, G. Chanvillard, Retention of the mechanical performances of Ductal®
543 specimens kept in various aggressive environments, in: Fib — Symp. 2004, Avignon,
544 26-28 April, 2004, 2004.

545 [11] N. ter Heide, E. Schlangen, Selfhealing of early age cracks in concrete, in: S. van der
546 Zwaag (Ed.), Proc. First Int. Conf. Self Heal. Mater., Springer, Noordwijk aan Zee, 18-
547 20 April 2007, 2007: pp. pp.1–12.

548 [12] N. ter Heide, Crack healing in hydrating concrete, Msc Thesis, Delft University of
549 Technology, 2005.

550 [13] S.J. Lokhorst, Deformational behavior of concrete influenced by hydration related
551 changes of the microstructure, Research Report, Delft University of Technology,
552 1999.

553 [14] E.A.B. Koenders, Simulation of volume changes in hardening cement-based
554 materials, PhD Thesis, Delft University Press, 1997.
555 http://repository.tudelft.nl/view/ir/uuid%3A1dbcb7fb-3f8f-466b-8517-b2235ad4912f/.

[15] K. van Breugel, Simulation of hydration and formation of structure in hardening cement-based materials. PhD Thesis, Delft University Press, 1991.

[16] H. Huang, G. Ye, D. Damidot, Characterization and quantification of self-healing behaviors of microcracks due to further hydration in cement paste, Cem. Concr. Res. 52 (2013) 71–81. doi:10.1016/j.cemconres.2013.05.003.

[17] J.C. Remmers, R. de Borst, Numerical modelling of self healing mechanisms, in: S. van der Zwaag (Ed.), Self Heal. Mater. SE - 17, Springer Netherlands, 2008: pp. pp.365–380. doi:10.1007/978-1-4020-6250-6_17.

[18] B. Hilloulin, F. Grondin, M. Matallah, A. Loukili, Modelling of autogenous healing in ultra high performance concrete, Cem. Concr. Res. 61-62 (2014) 64–70. doi:10.1016/j.cemconres.2014.04.003.

[19] R. Lewis, B. Schrefler, Finite Element Method in the deformation and consolidation of porous media, second ed., John Wiley & Sons, Chichester, 1998.

[20] D. Gawin, F. Pesavento, B.A. Schrefler, Hygro-thermo-chemo-mechanical modelling of concrete at early ages and beyond. Part I: hydration and hygro-thermal phenomena, Int. J. Numer. Methods Eng. 67 (2006) 299–331. doi:10.1002/nme.1615.

[21] A.S. Chitez, Coupled thermo-hygro-chemical modelling of self-healing processes in cementitious materials, PhD Thesis, Cardiff University, 2014.

[22] A.S. Chitez, A.D. Jefferson, Porosity development in a thermo-hygral finite element model for cementitious materials, Cem. Concr. Res. 78 (2015) 216–233. doi:10.1016/j.cemconres.2015.07.010.

[23] H.M. Jennings, Refinements to colloid model of C-S-H in cement: CM-II, Cem. Concr. Res. 38 (2008) 275–289. doi:10.1016/j.cemconres.2007.10.006.

[24] A.C.A. Muller, K.L. Scrivener, A.M. Gajewicz, P.J. McDonald, Use of bench-top NMR to measure the density, composition and desorption isotherm of C-S-H in cement paste, Microporous Mesoporous Mater. 178 (2013) 99–103. doi:10.1016/j.micromeso.2013.01.032.

[25] A.C.A. Muller, K.L. Scrivener, A.M. Gajewicz, P.J. McDonald, Densification of C-S-H measured by 1H NMR relaxometry, J. Phys. Chem. C. 117 (2013) 403–412. doi:10.1021/jp3102964.

[26] A.C.A. Muller, K.L. Scrivener, J. Skibsted, A.M. Gajewicz, P.J. McDonald, Influence of silica fume on the microstructure of cement pastes: New insights from 1H NMR relaxometry, Cem. Concr. Res. 74 (2015) 116–125. doi:10.1016/j.cemconres.2015.04.005.

[27] T.C. Powers, T.L. Brownyard, Studies of the physical properties of hardened portland cement paste, PCA Bull. Portl. Cem. Assoc. 43 (1948) 1–356.

[28] R.F. Feldman, Helium flow characteristics of rewetted specimens of dried hydrated Portland cement paste, Cem. Concr. Res. 3 (1973) 777–790. doi:10.1016/0008-8846(73)90011-2.

595 [29] K. Fujii, W. Kondo, Kinetics of the hydration of tricalcium silicate, J. Am. Ceram. Soc.
596 54 (1974) 492–497. doi:10.1016/j.jcis.2011.08.010.

597 [30] O. Bernard, F.-J. Ulm, E. Lemarchand, A multiscale micromechanics-hydration model
598 for the early-age elastic properties of cement-based materials, Cem. Concr. Res. 33
599 (2003) 1293–1309. doi:10.1016/S0008-8846(03)00039-5.

600 [31] T.C. Powers, The physical structure of Portland cement paste, in: H.F.W. Taylor, C.
601 Ogburn, S. Fuller, J. Chandler, T. Hardin (Eds.), Chem. Cem., Academic Press,
602 London, 1964: pp. pp.391–416.

603 [32] D.R. Gardner, A.D. Jefferson, R.J. Lark, An experimental, numerical and analytical
604 investigation of gas flow characteristics in concrete, Cem. Concr. Res. 38 (2008) 360–
605 367. doi:10.1016/j.cemconres.2007.10.001.

606 [33] M. Hassanizadeh, W.G. Gray, General conservation equations for multi-phase
607 systems: 1. Averaging procedure, Adv. Water Resour. 2 (1979) 131–144.
608 doi:10.1016/0309-1708(79)90025-3.

609 [34] M. Hassanizadeh, W.G. Gray, General conservation equations for multi-phase
610 systems: 3. Constitutive theory for porous media flow, Adv. Water Resour. 3 (1980)
611 25–40. doi:10.1016/0309-1708(80)90016-0.

612 [35] D. Gawin, C.E. Majorana, B.A. Schrefler, Numerical analysis of hygro-thermal
613 behaviour and damage of concrete at high temperature, Mech. Cohesive-Frictional
614 Mater. 4 (1999) 37–74. doi:10.1002/(SICI)1099-1484(199901)4:1<37::AID-
615 CFM58>3.0.CO;2-S.

616 [36] V. Baroghel-Bouny, Water vapour sorption experiments on hardened cementitious
617 materials. Part II: Essential tool for assessment of transport properties and for
618 durability prediction, Cem. Concr. Res. 37 (2007) 438–454.
619 doi:10.1016/j.cemconres.2006.11.017.

620 [37] P.L.J. Domone, J.M. Illston, Construction materials: their nature and behaviour, fourth
621 ed., Spon Press, London, 2010.

622 [38] A.K. Schindler, K.J. Folliard, Heat of hydration models for cementitious materials, ACI
623 Mater. J. 102 (2005) 24–33. doi:10.14359/14246.

624 [39] A.M. Neville, J.J. Brooks, Concrete Technology, Pearson Education Ltd., Singapore,
625 2003.

626 [40] D. Damidot, B. Lothenbach, D. Herfort, F.P. Glasser, Thermodynamics and cement
627 science, Cem. Concr. Res. 41 (2011) 679–695.
628 doi:10.1016/j.cemconres.2011.03.018.

629 [41] W. Chen, Z.H. Shui, H.J.H. Brouwers, A computed-based model for the alkali
630 concentrations in pore solution of hydrating Portland cement paste, in: Excell. Concr.
631 Constr. through Innov. - Limbachiya Kew, 2009.

632 [42] M. Koniorczyk, D. Gawin, Heat and Moisture Transport in Porous Building Materials
633 Containing Salt, J. Build. Phys. 31 (2008) 279–300. doi:10.1177/1744259107088003.

634 [43] M. Koniorczyk, Modelling the phase change of salt dissolved in pore water -
635 Equilibrium and non-equilibrium approach, Constr. Build. Mater. 24 (2010) 1119–
636 1128. doi:10.1016/j.conbuildmat.2009.12.031.

637 [44] H.F.W. Taylor, Cement chemistry, second ed., Thomas Telford, London, 1997.

638 [45] W. Kurdowski, Cement and Concrete Chemistry, in: Cem. Concr. Chem., 2014: pp.
639 pp.533–583. doi:10.1007/978-94-007-7945-7.

640 [46] A. Aliko-Benítez, M. Doblaré, J.A. Sanz-Herrera, Chemical-diffusive modeling of the
641 self-healing behavior in concrete, Int. J. Solids Struct. 69-70 (2015) 392–402.
642 doi:10.1016/j.ijsolstr.2015.05.011.

643 [47] H. Huang, G. Ye, Simulation of self-healing by further hydration in cementitious
644 materials, Cem. Concr. Compos. 34 (2012) 460–467.
645 doi:10.1016/j.cemconcomp.2012.01.003.

646 [48] V. Lagneau, J. van der Lee, Operator-splitting-based reactive transport models in
647 strong feedback of porosity change: The contribution of analytical solutions for
648 accuracy validation and estimator improvement, J. Contam. Hydrol. 112 (2010) 118–
649 129. doi:10.1016/j.jconhyd.2009.11.005.

650 [49] RILEM 2003: Early Age Cracking in Cementitious Systems - Report of RILEM
651 Technical Committee 181-EAS - Early age shrinkage induced stresses and cracking
652 in cementitious systems, Edited by A. Bentur, 2003.

653 [50] K. Van Tittelboom, H. Rahier, N. De Belie, E. Gruyaert, Influence of mix composition
654 on the extent of autogenous crack healing by continued hydration or calcium
655 carbonate formation, Constr. Build. Mater. 37 (2012) 349–359.
656 doi:10.1016/j.conbuildmat.2012.07.026.

657 [51] B. Hilloulin, D. Hilloulin, F. Grondin, A. Loukili, N. De Belie, Mechanical regains due to
658 self-healing in cementitious materials: Experimental measurements and micro-
659 mechanical model, Cem. Concr. Res. 80 (2016) 21–32.
660 doi:10.1016/j.cemconres.2015.11.005.

661 [52] M. Koniorczyk, Salt transport and crystallization in non-isothermal, partially saturated
662 porous materials considering ions interaction model, Int. J. Heat Mass Transf. 55
663 (2012) 665–679. doi:10.1016/j.ijheatmasstransfer.2011.10.043.

664 [53] R.D. Davies, Micromechanical modelling of self-healing cementitious materials, PhD
665 Thesis, Cardiff University, 2014.

666 [54] E. Gruyaert, P. Van Den Heede, N. De Belie, Carbonation of slag concrete: Effect of
667 the cement replacement level and curing on the carbonation coefficient - Effect of
668 carbonation on the pore structure, Cem. Concr. Compos. 35 (2013) 39–48.
669 doi:10.1016/j.cemconcomp.2012.08.024.

670 [55] M. Koniorczyk, D. Gawin, Modelling of salt crystallization in building materials with
671 microstructure - Poromechanical approach, Constr. Build. Mater. 36 (2012) 860–873.

672 [56] R. Cerny, P. Rovnonikova, Transport processes in concrete, Spoon Press, London,
673 2002.

[57] D. Gawin, F. Pesavento, B.A. Schrefler, Modeling of cementitious materials exposed to isothermal calcium leaching, considering process kinetics and advective water flow. Part 1: Theoretical model, Int. J. Solids Struct. 45 (2008) 6221–6240. doi:10.1016/j.ijsolstr.2008.07.010.

[58] V. Baroghel-Bouny, M. Mainguy, T. Lassabatere, O. Coussy, Characterization and identification of equilibrium and transfer moisture properties for ordinary and high-performance cementitious materials, Cem. Concr. Res. 29 (1999) 1225–1238. doi:10.1016/S0008-8846(99)00102-7.

[59] D. Gardner, A. Jefferson, A. Hoffman, Investigation of capillary flow in discrete cracks in cementitious materials, Cem. Concr. Res. 42 (2012) 972–981. doi:10.1016/j.cemconres.2012.03.017.

[60] N.J. Carino, H.S. Lew, The maturity method: from theory to application, in: P.C. Chang (Ed.), Struct. 2001, American Society of Civil Engineers, Washington D.C., 2001: pp. pp.1–19. doi:10.1061/40558(2001)17.

[61] S. Mindess, J.F. Young, D. Darwin, Concrete, Prentice Hall PTR, Upper Saddle River, 2003.

[62] H.M. Jennings, J.J. Thomas, Materials of Cement Science Primer: The Science of Concrete, Infrastructure Technology Institute for TEA, 2009. http://www.iti.northwestern.edu/publications/utc/tea-21/FR-5-Jennings-Thomas.pdf.

[63] P.D. Tennis, H.M. Jennings, A model for two types of calcium silicate hydrate in the microstructure of Portland cement pastes, Cem. Concr. Res. 30 (2000) 855–863. doi:10.1016/S0008-8846(00)00257-X.

[64] R. Berliner, M. Popovici, K.W. Herwig, M. Berliner, H.M. Jennings, J.J. Thomas, Quasielastic neutron scattering study of the effect of water-to-cement ratio on the hydration kinetics of tricalcium silicate, Cem. Concr. Res. 28 (1998) 231–243. doi:10.1016/S0008-8846(97)00260-3.

[65] S.C. McCutcheon, J.L. Martin, T.O.J. Barnwell, Water quality, in: D.R. Maidment (Ed.), Handb. Hydrol., McGraw-Hill, 1993: pp. pp.346–414.

[66] D. Gawin, F. Pesavento, B.A. Schrefler, What physical phenomena can be neglected when modelling concrete at high temperature? A comparative study. Part 1: Physical phenomena and mathematical model, Int. J. Solids Struct. 48 (2011) 1927–1944. doi:10.1016/j.ijsolstr.2011.03.004.

[67] D. Gawin, M. Wyrzykowski, F. Pesavento, Modeling Hygro-thermal Performance and Strains of Cementitious Building Materials Maturing in Variable Conditions, J. Build. Phys. 31 (2008) 301–318. doi:10.1177/1744259108089992.

[68] M.V.G. de Morais, B. Bary, G. Ranc, S.D. Pont, S. Durand, Comparative analysis of coupled Thermo-Hydro-Mechanical models for concrete exposed to moderate temperatures, Numer. Heat Transf. Part A Appl. 55 (2009) 654–682. doi:10.1080/10407780902821516.

713 [69] M.T. Van Genuchten, A closed form equation for predicting the hydraulic conductivity
714 of unsaturated soils, Soil Sci. Soc. Am. J. 44 (1980) 892–898.
715 doi:10.2136/sssaj1980.03615995004400050002x.

716 [70] N.E. Edlefsen, A.B.. Andersen, Thermodynamics of soil moisture, Hilgaria. 15 (1943)
717 1–298. doi:10.3733/hilg.v15n02p031.

718 [71] P.J. Cleall, An investigation of the thermo/hydraulic/mechanical behaviour of
719 unsaturated soils, including expansive clays, PhD Thesis, Cardiff University, 1998.

720 [72] J. Bear, Y. Bachmat, Introduction to modeling of transport phenomena in porous
721 media, Kluwer Academic Publishers, Dordrecht; Boston, 1991.

722